TECHNICAL NOTES

NATIONAL ADVISORY COMMITTEE FOR AERONAUTICS

No. 870

STRESS ANALYSIS OF MONOCOQUE FUSELAGE BULKHEADS BY THE PHOTOELASTIC METHOD

By Benjamin F. Ruffner
Oregon State College

Washington
December 1942

NATIONAL ADVISORY COMMITTEE FOR AERONAUTICS

TECHNICAL NOTE NO. 870

STRESS ANALYSIS OF MONOCOQUE FUSELAGE BULKHEADS BY THE PHOTOELASTIC METHOD

By Benjamin F. Ruffner

SUMMARY

An investigation was made to determine the possibility of using the photoelastic method for the stress analysis of bulkheads in monocoque structures. The method was applied to several typical bulkheads including a circular ring with floor beam, a circular ring attached to the main wing spar, and a flying-boat bulkhead. Methods for the construction of models and test technique are given. Tests of circular ring models were made to determine the effect of the skin thickness on the model results. Correction factors for the elimination of skin effect are included. The results indicate that the photoelastic method is quite accurate. The method is recommended for use where bulkheads with a large number of redundancies are present.

INTRODUCTION

Since the monocoque and the semimonocoque types of construction have come into general use, many analytical methods of stress analysis of stiffening rings and bulkheads have been published. The simplest type, the circular ring of constant bending stiffness, offers some analytical difficulty although many special cases of loading for this type have been treated (references 1, 2, and 3). Certain general methods of analysis of noncircular, nonuniform rings have been discussed (references 4 and 5), but the use of these methods involves either extremely complicated analysis or laborious graphical methods. In actual aircraft structures circular ring bulkheads of uniform section are usually not the most efficient design.

In many actual cases the analysis of the bulkheads is further complicated by the attachment of floor beams, wing

beams, and other members. These members, if tied into the bulkhead, tend to increase the number of redundancies. This increase affects the stress distribution in the bulkhead and greatly complicates the problem of analysis. Although some of the analytical methods discussed in the references may be used in the general case, they are so laborious and the possibility of error is so great that they are impractical for use in routine design.

Several years ago it was pointed out (reference 6) that the photoelastic method could be used for the solution of this bulkhead problem. The purpose of the investigation reported herein is to develop a technique for the photoelastic solution of the problem. The present report deals with the construction of the models, the methods of loading, certain short cuts in the analysis of bending moment that seem to be justified, and the effect of certain variables on the accuracy of the test method.

APPARATUS

The apparatus used in the tests reported is located in the photoelastic laboratory at Oregon State College. The light source on the photoelastic polariscope consists of a type H-4 mercury vapor lamp. Light filters are used to transmit the green light, in the mercury vapor spectrum, having a wave length of 5460 angstrom units. The polarized field in which models may be placed is 6¼ inches in diameter. The image of the stressed model is focused either on a screen or on a photographic film. The light in the working field is circularly polarized by means of a 6¼-inch sheet of Polaroid and a 6¼-inch one-quarter wave plate. The analyzer units consist of another 6¼-inch one-quarter wave plate and another 6¼-inch sheet of Polaroid. A photograph of the polariscope is shown in figure 1.

Material selected for the construction of the models was Bakelite BT-61-893. This material may be easily machined, polished, and annealed and has a high elastic limit and a high stress-optic coefficient.

CONSTRUCTION AND MOUNTING OF MODELS

In order to obtain good results from photoelastic tests, it is important that the models being tested be properly designed and constructed. The faces of the model perpendicular to the path of the light in the polariscope should be true plane surfaces, free from scratches, and highly polished. When tested, the models should, in the unloaded condition, be free from initial stress or its optical equivalent. Whenever possible the model should be geometrically similar to the actual structure. In many models, however, geometric similarity is not possible because of the requirement that the faces of the model perpendicular to the light path be parallel.

In the present investigation of bulkheads or stiffener rings in monocoque structures, the largest stresses in these rings are those due to bending. If the model is so designed as to represent the proper distribution of bending moment in the bulkheads, the results obtained from the model tests will be satisfactory. Many full-scale bulkheads and stiffener rings are constructed of built-up sections, I sections, T sections, or other extruded sections of various shapes. In the design of models of these full-scale structures it is usually simplest to have the model of constant thickness and to vary the depth of the cross section at each point in such a way that the ratio of the bending stiffness of any section of the model to bending stiffness of the corresponding full-scale section is the same for all cross sections. The shape of the neutral axis on the model should then be geometrically similar to the full-scale original. The bending stiffness will be designated by EI, which is the product of the modulus elasticity and the moment of inertia of the section in the plane of bending. If the model is designed in this fashion, the distribution of bending moment in the model will be very close to the distribution of bending moment in the full-scale structure.

If extremely heavy and stiff bulkheads are being tested in which the shear stresses are large as compared with the stresses due to bending, then it may be necessary to build a model of varying thickness. In most practical cases, however, such construction may be avoided.

The material for the model, Bakelite BT-61-893, is available in sheets of various thicknesses from 1/4 inch

to 1/2 inch. The procedure used for the construction of the models was as follows:

1. The outlines of the model were accurately laid out on the bakelite sheet and were scribed lightly on the surface.

2. The model was cut to within about 3/32 or 1/8 inch of the scribed lines on a jigsaw. In this operation a fine, sharp saw was used and the material was cut slowly, care being taken that the material did not become heated.

3. The faces of the model were sanded and polished. A power sander was used until the surface was fairly smooth and the model was of constant thickness. The model was then polished on a polishing lap; levigated alumina was used as a polishing abrasive.

4. The model was annealed after polishing to remove any initial stress or optical birefringence. The annealing oven used holds a temperature of 260° F for 12 hours and then cools at the rate of 16° F per hour down to room temperature.

5. Sometimes, after annealing, a small amount of polishing was necessary.

6. The model was cut to final dimensions by one of the methods discussed in the following paragraphs. The final model should have its faces parallel, its corners square and sharp, and its faces free of scratches.

The model may be cut to final shape with many types of machine tools. It is important to be sure that tools are sharp and that final finishing cuts are very light in order not to introduce machining stresses into the model.

The circular rings shown in figure 3 were all cut on a small bench lathe. The model was first cemented to a smooth wood face plate, using Dennison's or Duco household cement or similar adhesive to hold the model on the face plate. Under no conditions should the model be held directly in the jaws of a chuck because stresses may be introduced. The model was cut with a sharp tool to final size. The last few cuts did not remove more than 1/1000 of an inch. The model was then removed from the wood face plate by soaking in acetone, which dissolves the adhesive used but does not affect the bakelite or the polish on the

surface. Once the model has been cut, it should not be polished again as polishing at this point may round the corners and interfere with the determination of edge stresses. The model was tested as soon as possible after completion as effects of birefringence begin to appear on the model a short time afterward. A photograph of a circular ring model set up in the lathe is shown in figure 4.

For cutting models having straight edges, the use of a milling machine is quite satisfactory. Here again, however, models should be cemented to a wood block rather than held directly in a vise. It is important to use a sharp cutter and to take small finishing cuts.

For cutting models such as the flying-boat bulkhead, model 7 (fig. 3), a vertical mill or shaper is very convenient. A metal template 7-T (fig. 3) was first cut out. The drawing of the bulkhead model and template is shown in figure 5. This template was 0.032 inch undersize on all edges. In figure 6 are shown the method of attaching the model to a wood face plate and the method of attaching the metal template to the bakelite stock. A hardened and ground steel collar was fitted over the milling cutter and adjusted to ride against the template. The thickness of the wall of this collar was the same as the amount that the template was cut under size, in this case 0.032 inch. In some cases it may be necessary to feed the model into the cutter by hand. This method is quite satisfactory if care is taken not to feed too rapidly. If possible, the wood face plate should be mounted in a compound rest. Feeding screws should be used. Figure 7 shows the model set up in the vertical mill. The wood and template may be removed from the model by soaking in acetone in the same manner as previously described.

With the exception of a few preliminary tests on the circular rings, all models were supported as bulkheads in monocoque structures. Loads were applied directly to these bulkheads and the reactions were taken through the thin skin. For test purposes it was found most convenient to mount the bulkheads at one end of a cantilever tube as shown in figures 8, 9, and 10. Several materials for the skin were tried, including cardboard, fiber board, and celluloid. All these materials can be used but thin sheet celluloid was found to be by far the most satisfactory. In the construction of these models several requirements must be met: First, the light rays in the polariscope

must pass through the model unobstructed by the skin or supports. Second, the loads must be applied to the bulkhead. Third, the mounting must be rigid in order that the deflections under load are not so great as to move the model into a position where the light will be obstructed.

In order to keep the light path free so that edge stresses on the model could be determined readily, a slight taper, as shown in figure 9, was introduced into the skin support of the model. The amount of taper was varied on several tests; about $2\frac{1}{2}^{\circ}$ seems to be the most satisfactory amount. The procedure for constructing the mounting for the model was as follows:

1. A drawing of the support was made.

2. A drawing of an accurate development of the skin surface was made which was used as a pattern for cutting the celluloid skin. Edges of this celluloid skin were welded together as a butt weld with the inner surface flush. A cover plate of celluloid was used. The actual weld was made by moistening both the skin and the cover plate with acetone and clamping in place till dry.

3. A wood form was cut out to hold the celluloid skin. The skin was cemented to this form with Dennison's or Duco household cement, as shown in figure 9.

4. The bakelite model was then cemented into the skin with the same adhesive. A completed model of the elliptic ring is shown in figure 8.

In figure 10 is shown a circular ring model set up in the polariscope for test.

TESTS OF CIRCULAR RINGS WITH DIAMETRICAL LOADS

The problem of analysis of a bulkhead ring consists fundamentally in determining the forces and moments at one or several sections. If this procedure is followed, forces and moments at other sections of the ring may be determined by applying the principles of statics. In many practical cases, when the bulkhead is supported by a varying shear reaction in the skin to which it is attached, the problem in statics involved, even after forces and moments at one section are known, is still difficult to solve. It was

believed that, if the stresses at the inner and outer fibers of the bulkhead were known, the moments could be calculated with sufficient accuracy if linear distribution of the bending stress across the section were assumed. From a photoelastic test it is a simple matter to determine the boundary stresses. It is well known that, if the beam is curved, the assumption of linear stress distribution does not apply; however, it may be demonstrated that, as the ratio of the depth of the beam to the radius of the curvature of the neutral axis becomes small, linear stress distribution is approached. A series of tests was made to determine what accuracy could be obtained in practical problems if linear stress distribution were assumed.

In a beam subjected to bending, the shear force perpendicular to the neutral axis is zero at a section of maximum moment; consequently, at such a section the principal stresses are perpendicular and parallel to the neutral axis and, furthermore, the principal stress perpendicular to the neutral axis is zero if the boundaries are unloaded (references 7 and 8). In a field of circularly polarized light, each interference fringe appearing on the image of the photoelastic model represents the locus of points where the difference between the principal stresses is equal to a constant times the fringe order (references 7 and 8). At a section of maximum moment, therefore, the bending stresses may be computed directly from the fringe photograph and a plot of bending stress against depth of beam may very readily be made at this one section. If the distribution of stress with depth of beam is known, the bending moment due to these stresses may be accurately determined by a graphical integration. In order to determine the difference between the exact bending moment and the approximate value obtained by assuming linear distribution, a series of tests was run on four circular ring models of constant EI. These rings were subjected to concentrated loads on the diameters. Models were set in the field of the polariscope, loads were applied, and a photograph of the fringe pattern was taken. In figure 11 model 4 is shown set up for diametrical load test. In figure 12 is shown the fringe pattern for model 4 loaded with a diametrical load of 51.3 pounds.

In reference 1 the following formula (in substantially the same form) is given for the computation of bending moments in a circular ring of constant EI subjected to diametrically opposed loads:

$$\frac{M}{WR_M} = -\left(\frac{1}{\pi} - \frac{1}{2}\sin\theta\right)$$

where

M bending moment at any cross section of ring, pound-inches

θ variable angle (See fig. 9.)

W load applied to ring, pounds

R_M mean radius, inches

This formula was derived on the assumption that a linear stress distribution existed across the depth of the ring section, that the loaded ring is still circular in shape, and that the strain energy due to the axial loads and shear forces is negligible. The formula is included here for purposes of comparison of the results obtained from the photoelastic tests with the approximate theoretical solution. Where the inner surface of the ring is in tension, the moment is assumed to be positive. The load is assumed to be positive when it acts outwardly from the center.

In order to determine the value of the principal stress difference corresponding to any particular fringe, it is necessary to know, for the material and wave length of light used, the value of the principal stress difference per fringe order. In order to obtain this value, a rectangular beam model 0.363 inch deep and 0.300 inch thick was cut from the same material that was used for the rings. This model was supported as a simple beam of 4-inch span and was loaded with equal loads 1.0 inch from each support. The equal loads were each 10.24 pounds, which gave a maximum constant bending moment between the loads of 10.24 inch-pounds. The stress in the outer fibers at a distance c from the neutral axis at the center section is given by the formula

$$\sigma = \frac{Mc}{I} = \frac{10.24 \times 0.1815}{0.001195} = 1555 \text{ pounds per square inch.}$$

From the fringe photograph of this calibration beam (fig. 13) the fringe order at the outer fibers was determined to be 5.15. This value gives a principal stress differ-

ence of $\sigma_1 - \sigma_2 = 302\ n$, where n is the fringe order for the model of 0.300-inch thickness. Since, for a given material and wave length of light, the stress per fringe order is inversely proportional to the thickness, the material used may then be considered to have a stress per fringe order per inch thickness equal to $K = 90.6$ pounds per square inch per inch thickness.

In table I are given dimensions of circular ring models. The symbols used for the dimensions are defined in figure 2. In table II are shown the loads and moments at the point $\theta = 90^{\circ}$ for the four circular ring models tested. The moments were computed by two different methods. The first method assumed that the stress distribution across the section was linear. On the basis of this assumption, the tensile stress is

$$s_t = \frac{Mc}{I} + \frac{P}{A}$$

and the compressive stress

$$s_c = \frac{Mc}{I} - \frac{P}{A}$$

where P is defined as the axial force and A is the cross-sectional area of the ring. The sum of the tensile and compressive stresses is, then,

$$s_c + s_t = \frac{2Mc}{I}$$

or

$$M = \frac{I(s_c + s_t)}{2c}$$

Since at the outer fiber one of the principal stresses is zero and the other is equal to either the tensile or compressive stress, then

$$s_c = \frac{k\ n_c}{h}$$

$$s_t = \frac{k\ n_t}{h}$$

where n_c is the fringe order at the outer fiber on the

compression side and n_t is the fringe order at the outer fiber on the tension side. Therefore,

$$M = \frac{I\ k\ (n_c + n_t)}{2ch}$$

or

$$M = \frac{d^2\ k\ (n_c + n_t)}{12} \qquad (1)$$

From equation (1) it is apparent that the bending moment may be calculated immediately from the photographic pattern if the fringe orders on the compression and tension sides of the beam are known. In order to determine these fringe orders, the fringe order may be plotted against the depth of the beam and values of fringe orders at the boundaries may then be picked from the curve. Figure 14 shows this plot for the points $\theta = 90^\circ$ and $\theta = 270^\circ$ for the test made on model 4. This plot was made by measuring the location of the fringes on the photograph shown in figure 12. Results of these measurements are given in table III. If great accuracy is not desired, it is unnecessary to plot the fringe order against depth. In many cases the fringe orders may be determined merely by inspection of the photograph. By inspection the fringe order can be determined within ± 0.3 of a fringe order. If equation (1) is applied to the test on model 4,

$$M = \frac{(0.495)^2\ (90.6)\ (4.44 + 6.61)}{12} = 20.55$$

This equation gives a value of M/WR_M as follows:

$$\frac{M}{WR_M} = \frac{20.55}{51.3\ (2.002)} = 0.200$$

At the section of maximum moment at the points $\theta = 90^\circ$ and $\theta = 270^\circ$, as shown in figure 12, the stress across these sections may be computed as in table III and plotted as in figure 15. These stresses are produced by combined action of bending and axial loads. The average stress across the cross section is given by the mean ordinate of the curve. The point in the cross section where the combined stress is equal to the mean ordinate is the point of location of the neutral axis.

The actual bending moment may be computed at these points by finding the value

$$M = h \int_0^d \sigma' \, y' \, dy$$

where σ' is the bending stress and y' is the distance from the neutral axis. In table IV values of $\sigma' y'$ are given. If the product $\sigma' y'$ is plotted against the depth of the beam as in figure 16, the area under the curve is the value under the integral in the equation for M. Bending moments at the maximum points were computed for all four rings tested with diametrical loads, and the values are given in table II in the column headed "M/WR_M (computed from actual stress distribution)."

The average value of M/WR_M at $\theta = 90^\circ$ for the four rings was 0.2004 when the simplifying assumption of linear stress distribution was made. The average value obtained by the more lengthy graphical method, which is theoretically the more accurate, was 0.2028. The difference between these values is about 1 percent, which is less than the experimental error normally present in any photoelastic test. In view of the excellent agreement between these two methods, it is believed that the use of the assumption of linear stress distribution is fully justified and this method was used in all subsequent tests.

The assumption of linear stress distribution makes the determination of bending moments possible at all sections merely by determining the boundary stresses. If these boundaries are unloaded, the boundary stresses are principal stresses and one of them is zero. Consequently, a knowledge of the fringe orders at the boundaries immediately gives the combined stress due to bending and axial load and the bending moments may be computed by equation (1). The other method is applicable only to sections of maximum moment; it is fortunate, therefore, that the linear assumption is justified.

In figure 17 are shown curves of M/WR_M against θ calculated from Miller and Wood's theoretical solution (reference 1) and from the fringe photograph of figure 12 by use of the assumption of linear distribution. The shapes of the curves show excellent agreement. The maximum dif-

ference between the two curves occurs at the point of maximum positive moment. The difference is about 10 percent of the value obtained from the photoelastic tests. Of the two, the results obtained from the photoelastic tests should be the more accurate because the theoretical values are based upon a strain-energy solution in which the strain energies due to shear and axial loads are neglected.

TESTS OF CIRCULAR RINGS SUPPORTED AS BULKHEADS

Both on the models and in actual monocoque structures the thin skin attached rigidly to the bulkhead will relieve the bending moment in the bulkhead. The skin acts as a thin flange on a beam. The bending moments in the bulkhead will depend both on the thickness of the skin and the rigidity of this shell structure in resisting deformation of the bulkhead. In the model tests, since the wood support was extremely rigid as compared with the bulkhead model, this stiffness might be considerably greater than in a full-scale structure. This series of tests was run on several circular rings of constant cross section to determine the effect of variation of skin thickness and length of support l on the bending moments taken by the bulkhead models. The loads on these rings were applied as shown in figure 9. Positive bending moments were assumed to produce tension in the inner edge of the ring.

When the rings were loaded in this manner, the maximum bending moments in the rings occurred at approximately $\theta = 75^{\circ}$. The values of the moments at $\theta = 75^{\circ}$ were computed for all tests as listed in table V. In the tests of the diametrically loaded rings previously discussed, the boundaries of the model except at the point of application of the concentrated loads were free of external stress and, as a result, a determination of the tensile or compressive stresses at the boundaries could be obtained directly from a knowledge of the fringe orders. In the series of tests with the rings supported by shear reactions in the skin, the shear stress at the boundary of the bakelite models is not zero. In figure 18 is shown Mohr's circle diagram of stress for the edge of the model attached to the skin. The stress s_t is the tensile or compressive stress at the edge of the ring; s_s is the shear stress, due to the skin, on the outer boundary of the ring; and $\sigma_1 - \sigma_2$ is the difference between the principal stresses and is equal to

a constant times the fringe order at the boundary. If the angle ϕ (fig. 18) is small, $\cos \phi$ is equal to approximately 1.00, and it may be assumed with negligible error that the tensile stress s_t is equal to a constant times a fringe order.

In order to find out whether the angle ϕ is small, a quantitative analysis of the values s_s and s_t was made as follows: From reference 2,

$$s_s = \frac{W \sin \theta}{\pi R h}$$

and

$$M = \frac{WR}{2\pi}\left[1 - (\pi - \theta) \sin \theta + \frac{1}{2} \cos\right]$$

where R corresponds to R_M as used in this paper. Therefore,

$$s_t = \frac{Mc}{I} = \frac{6M}{hd^2} = \frac{6WR}{2\pi h d^2}\left[1 - (\pi - \theta) \sin \theta + \frac{1}{2} \cos \theta\right]$$

From the Mohr circle diagram in figure 18, $s_t = (\sigma_1 - \sigma_2) \cos \phi$. Also, from figure 18,

$$\phi = \tan^{-1} \frac{2s_s}{s_t}$$

therefore

$$\tan \phi = \frac{3W \sin \theta \, (hd^2\pi)}{\pi R h \, (3WR)\left[1 - (\pi - \theta) \sin \theta + \frac{1}{2} \cos \theta\right]}$$

or

$$\tan \phi = \frac{2}{3}\left(\frac{d}{R}\right)^2 \frac{\sin \theta}{\left[1 - (\pi - \theta) \sin \theta + \frac{1}{2} \cos \theta\right]}$$

In table VI values of $\tan \phi$ and $\cos \phi$ were computed for a value of $\frac{d}{R} = \frac{1}{4}$. This quantity represents the value for the deepest model tested. These values of $\tan \phi$ and $\cos \phi$ are plotted in figure 19. Except at the points where the moment is equal to zero, the factor $\cos \phi$ is

considered to be so little different from 1.00, particularly at the maximum moment, that s_t is equal to a constant times the principal stress difference $\sigma_1 - \sigma_2$. In view of the fact that s_t has such a value, all the moments were computed as though the boundary shear stress were equal to zero and the moments could be obtained in exactly the same way as in the tests of the rings under diametrical load.

In figure 20 is shown the photoelastic fringe pattern for model 4, test 5, with a load of 120 pounds and supported in a skin of 0.020 inch thickness. The fringe orders for all fringes must be known. These may be obtained by observing the formation of the fringes as the model is loaded. The location of the fringe orders at sections $\theta = \pm 75^\circ$ are given in table VII. In figure 21 is plotted the fringe order against distance from the outer edge of the model. The difference between the fringe orders on the outer and inner edges is $8.20 - (-4.80) = 13.00$. By counting the fringes and estimating the fringe order at the boundary, this same difference was determined to be 12.95. By use of equation (1)

$$\frac{M}{WR_M} = \frac{d^2k\,(n_c+n_t)}{12\,(WR_M)} = \frac{(0.0495)^2\,(90.6)\,(13.0)}{12\,(120)\,(2.002)} = 0.0995$$

In table V are given the results of the complete series of tests on circular rings mounted and loaded as shown in figure 9. In order that all results be put in nondimensional form, the moments were all divided by WR_M. The length l of the cantilever support was divided by D_M and the thickness of the celluloid skin t was divided by d. Results of all those tests were plotted as shown in figure 22. The series of curves for various values of l/D_M were faired as a family. These curves were then cross-plotted as shown in figure 23 in which the effective thickness t_e is defined by the equation

$$t_e = \frac{E_{celluloid}}{E_{bakelite}}\,(t)$$

The curves in figure 23 indicate that as the length of the cantilever support is increased, the value of the moment in the rings approaches asymptotic values at an l/D_M ratio of approximately 1.0. The effect of the skin on the

moments of the ring is quite large. In these tests the modulus of elasticity E of the celluloid skin is approximately 150,000 and the modulus of elasticity of the bakelite is 648,000.

In using the photoelastic method to determine the moments and forces in bulkhead models, it is recommended that all values of tests be corrected for the effect of the model skin and the length of support. If, for instance, a test of a model is made at an l/D_M ratio of 0.4 and a t/d ratio of 0.20, the moments in the model should then be corrected by the use of figure 24. In figure 24 the factor F is plotted against l/D_M for various values of t/d. This factor F may be written

$$F = \frac{M}{WR_M} \Bigg/ \frac{M_{t \to 0,\ l \to \infty}}{WR_M}$$

At the values mentioned, F is equal to 0.83. The moments obtained in the test model, therefore, should be divided by 0.83. Although this procedure will probably give values of M somewhat higher than would actually be obtained in practice, it is nevertheless conservative and it is probable that the skin effect on actual fuselages will be less than on the model.

In several of the tests made, the models were so loaded that the thin skin buckled and formed tension fields. On model 201, test 1, with a load of 16.05 pounds, the skin did not buckle. When the load was increased to 20.60 pounds, very definite waves were formed in the skin. The maximum values of M/WR_M, however, were very little different, being slightly less for the buckled condition. On model 3, test 1a, the skin was not buckled under a load of 72.70 pounds but was buckled under a load of 90.00 pounds. Again, the maximum moment was affected very little

In figure 25 curves are plotted showing the variation of moments with θ for a typical circular ring loaded as shown in figure 9. In table VIII complete data are given. The values of the fringe orders $n_c + n_t$ were obtained by estimating the fringe orders on the boundary of the model. Since the loading and the ring were were both symmetrical, the values were averaged at corresponding points on the

two sides of the ring. The values of M/WR_M were corrected by the use of the factor F in figure 24. Also plotted in figure 25 are theoretical values obtained by the use of equations in reference 2. As in the tests for diametrical loads, the maximum moments obtained from the test of the model are somewhat higher than those given by the theoretical solution.

From this series of tests, it appears that almost any convenient values may be selected for model dimensions, skin thicknesses, length of span, etc., and corrections can be made in accordance with the method outlined. It is recommended, however, that an average diameter of model of 3 to $3\frac{1}{2}$ inches, a cantilever span of about $1\frac{1}{2}$ inches, and a celluloid skin about 0.020 inch thick be used. These dimensions give a model of sufficient size to be easily worked and constructed.

TESTS OF TYPICAL BULKHEAD MODELS

Tests of Model 8

Model 8 represents a typical bulkhead composed of a floor beam attached to a circular ring. Dimensions of the model are shown in figure 26. The fringe pattern of the model loaded with a total load of 61.2 pounds is shown in figure 27. Some stress analysts have analyzed this structure on the assumption that the floor beam merely transferred the loads to the points of attachment of the floor beams to the rings. This assumption is not justified, however, as the stiffness of the floor beam has a marked effect on the distribution of stress in the ring as a whole.

For this beam

$$M/WR_M = \frac{d^2 k (n_c + n_t)}{12 (WR_M)} = 0.00412 (n_c + n_t)$$

$$\frac{l}{D_M} = \frac{1.70}{2.76} = 0.618$$

and

$$\frac{t}{d} = \frac{0.020}{0.215} = 0.093$$

From figure 24, F = 0.928. In table IX are shown the calculations for the values of M/WR_M at various points around the ring. The theoretical values in this table were obtained from an unpublished paper by Wayne Wiesner entitled "Monocoque Fuselage Braced Circular Ring Analysis", which was written in 1940 in competition for United Air Line Scholarship Awards. The value of M/WR_M in the floor beam itself between the loads is equal to 0.0642. Both sets of values, observed and theoretical, are plotted in figure 28.

This structure is an excellent example of the value of the photoelastic method. From an analytical standpoint, the structure has six redundancies. In using the photoelastic method, however, the number of redundancies does not complicate the analysis. Wiesner's theoretical solution applies only to structures where the moment of inertia of the ring is constant. The photoelastic method, however, can be applied just as easily whether or not the moment of inertia of the ring is constant.

Test of Model 6

The main wing beams of many airplanes are attached directly to a bulkhead. Model 6 (fig. 3) represents such a combination. In several airplanes having this type of arrangement, the ratio of the moment of inertia of the beam to the moment of inertia of the bulkhead ring was of the order of 1000 to 1200. In order to obtain a stiffness ratio this high in the model, brass plates were bolted to the sides of the bakelite spar to stiffen that part of the model. The model was tested at a ratio of EI of the beam to EI of the bulkhead ring of 1142. The dimensions of model 6, which is made of bakelite, are given in figure 28. The loads were applied a distance b from a center line in such a way that the bending moment at the intersection of the spar and the ring would represent the moments that would be obtained on a normal cantilever wing. Figure 29 shows the fringe pattern obtained on the ring with a total load W = 79.6 pounds. The value of M/WR_M for the ring is given by $M/WR_M = 0.00263 (n_c + n_t)$. The ratio l/D_M is 1.00, and the ratio t/d is 0.102. From figure 24 the factor F equals 0.93. The loads W/2 were applied at a distance $b/R_M = 2.50$ from the center line. In table X are shown the values of M/WR_M for this model. These values are plotted in figure 28. From these results

it is seen that the structure would be more efficient if the top of the ring were lightened as compared with the sections down near the wing root.

Test of Model 9

Many fuselage structures are elliptic rather than circular in section. A test was made of an elliptic ring model, model 9, to show application of the method to elliptic rings. The model was constructed by first laying out a metal template 0.032 inch under size on both the inner and the outer edges. The model was then cut in the same manner as the flying-boat-bulkhead model previously described. The major diameter of the neutral axis of the ellipse was 3.66 inches and the minor diameter was 2.70 inches. A nondimensional plot of moments for the circular rings was obtained by dividing the moment by the load times the radius. Since the radius of the circle may be considered as equal to $\sqrt{A/\pi}$, in order to obtain a nondimensional plot of the moments for the elliptic ring, the moments were divided by $W\sqrt{A/\pi} = \sqrt{a\,b}$, where a is the semimajor axis and b is the semiminor axis. In order to obtain a correction factor from figure 24, the l/D_M ratio was considered to be equal to $\frac{l}{2\sqrt{ab}} = \frac{1.13}{3.142} = 0.36$. The ratio t/d for this test was 0.067. Then, from figure 24, F = 0.92. In figure 30 is shown a drawing of the model and a definition of the angle . The fringe pattern for model 9 is shown in figure 31. In table XI are given the calculations for $\frac{M}{W\sqrt{ab}}$. These values are plotted in figure 30. It should be noted that these values will be applicable only, however, to an elliptic ring with a ratio a/b equal to $\frac{1.83}{1.35}$ or 1.355.

Test of Model 7

In figure 6 were shown the ordinates and a drawing of the flying-boat-bulkhead model 7. Also on this figure is shown a drawing of the brass template used for cutting the model. The neutral axis of this model is geometrically similar to the neutral axis on a typical full-scale flying-

boat bulkhead for which data were available. The dimension d of the model is such that the ratio between moments of inertia of any two sections on the model is the same as the ratio between moments of inertia of any two corresponding full-scale sections. In figure 32 is shown the model set up for test. Loads were applied to steel straps. Loads from the steel straps were distributed to rubber spacers which, in turn, distributed the loads to the model. The loading condition represents an equally distributed load over the bottom of the hull of 2.505 pounds per inch on the bottom, or a total load of 115.2 pounds. As for the case of the elliptic ring, in order to make a nondimensional plot, the moments were divided by the product $W\sqrt{A/\pi}$, where A is equal to the included area inside the neutral axis of the model. For this model, A = 8.70 square inches. The length of the cantilever support was 2.20 inches and the thickness of the skin was 0.020 inch. The value of $\frac{M}{W\sqrt{A/\pi}}$ was $0.393\ d^2\ (n_c + n_t)$. In figure 33 is shown the fringe pattern under the loading condition described. The calculations for determining the corrected values of $\frac{M}{W\sqrt{A/\pi}}$ for this model are given in table XII. As the depth of the cross section was not a constant, the value of t/d varied and, consequently, the factor F as determined from figure 24 also varied. The moment curve for this bulkhead is plotted in figure 34.

DETERMINATION OF SHEAR FORCES AND AXIAL LOADS IN THE BULKHEADS

The technique and the examples given have emphasized the method of determination of moments in the bulkheads. In general, if the moments are known at all sections and the external shear reaction in the skin is determined by the usual methods, from principles of statics the axial loads and shear forces in the bulkheads may be determined. The shear force at any section in the bulkhead, however, may also be obtained from the slope of the moment diagram. For instance, if the moment in the bulkhead is plotted against θ as in figure 17, the shear force S is equal to $\frac{dM}{R_M(d\theta)}$ or, in general, is equal to dM/ds, where s is the distance along the neutral axis of the bulkhead.

Axial loads at the sections of maximum moment may be determined by finding the component of average stress parallel to the neutral axis. In figure 15 combined stress due to bending moment and axial load is plotted against the depth of the bulkhead. The net area under this curve divided by the depth of the bulkhead d is equal to the unit stress produced by the axial load. This average stress multiplied by the cross-sectional area will give the axial load.

At sections where the moment is not a maximum, an estimate of the axial load may be obtained by assuming a linear distribution of bending stress and taking the average fringe order existing at the section. This average may be obtained by taking $\frac{n_t - n_c}{2}$. If at a given section the fringe order on the tension side is 6.0 and the fringe order on the compression side is 2.0, the average fringe order is then $\frac{6.0 - 2.0}{2.0} = 2.0$. The average stress s_{av} equals $k\left(\frac{n_t - n_c}{2h}\right)$ and the axial load P equals $s_a d$.

This method of determining the axial load may be considerably more in error than that used for the determination of moments. The determination of moments depends on the sum of the fringe orders whereas the axial load depends upon the difference; as a result, a small error in determining individual fringe order might cause considerable error in determining this difference. It is suggested that if axial loads are desired they be determined approximately by the method outlined and checked by use of the equations of statics using the values of moments previously determined.

CONCLUSIONS

1. It is believed that the photoelastic method of stress analysis discussed herein is readily applicable to the solution of the statically indeterminate problems involved in the stress analysis of bulkheads and that this method is more accurate than those analytical methods commonly used.

2. If the bending moments, the axial loads, and the shears are determined at every section in a bulkhead, the

stress-analysis problem involved is then merely to check to see if the full-scale bulkhead has sufficient moment of inertia and cross-sectional area to resist these known forces and moments.

Oregon State College,
Corvallis, Oreg., June 1942.

REFERENCES

1. Miller, Roy A., and Wood, Karl D.: Formulas for the Stress Analysis of Circular Rings in a Monocoque Fuselage. T.N. No. 462, NACA, 1938.

2. Ruffner, Benjamin F., Jr.: Monocoque Fuselage Circular Ring Analysis. Jour. Aero. Sci., vol. 6, no. 3, Jan. 1939, pp. 114-116.

3. Wise, Joseph A.: Analysis of Circular Rings for Monocoque Fuselages. Jour. Aero. Sci., vol. 6, no. 11, Sept. 1939, pp. 460-463.

4. Lundquist, Eugene E., and Burke, Walter F.: General Equations for the Stress Analysis of Rings. Rep. No. 509, NACA, 1934.

5. Hoff, N. J.: Stress Analysis of Rings for Monocoque Fuselages. Jour. Aero. Sci., vol. 9, no. 7, May 1942, pp. 245-251.

6. Ruffner, Benjamin F., Jr.: The Photoelastic Method as an Aid in Stress Analysis and Structural Design. Aero Digest, vol. 34, no. 4, April 1939, pp. 60, 61.

7. Frocht, Max M.: The Place of Photoelasticity in the Analysis of Statically Indeterminate Structures. Eng. Bull. Carnegie Inst. Tech., 1938.

8. Frocht, Max Mark: Photoelasticity. Vol. I. John Wiley & Sons, Inc., 1941.

TABLE I

DIMENSIONS OF CIRCULAR RING MODELS

[Symbols defined in fig. 2. All dimensions in in.]

Ring model	D_o	D_i	D_M	d	h
1	2.830	2.342	2.586	0.244	0.268
2	2.258	1.738	1.998	.260	.313
3	3.350	2.630	2.980	.360	.310
4	4.500	3.510	4.005	.495	.309
4a	4.458	3.482	3.970	.488	.293
401	4.335	3.629	3.982	.353	.262
301	3.284	2.742	3.013	.271	.268
201	2.188	1.846	2.017	.171	.269

TABLE II

RESULTS OF DIAMETRICAL LOAD TESTS

ON MODELS 1, 2, 3, AND 4

[Theoretical $M/WR_M = 0.1817$ (90°). Values of M/WR_M are average of values obtained at $\theta = 90^\circ$ and $\theta = 270^\circ$]

Model	Test	Load, W (lb)	Mean radius R_M (in.)	WR_M	M/WR_M (Linear stress distribution assumed)	M/WR_M (Computed from actual stress distribution)
1	(a)	16.00	1.293	20.68	0.2050	0.2120
2	3	27.30	.999	27.29	.1965	.1965
3	3	38.60	1.490	57.50	.2000	.2020
4	3	51.30	2.002	102.8	.2000	.2005

TABLE III

MEASUREMENT OF LOCATION OF FRINGES, FROM FIGURE 12

[Model 4; test 3; diametrical load, 51.3 lb; origin on outside boundary of ring; diameter of ring in photograph, 3.82 in.; actual diameter of ring, 4.50 in.; ratio of diameters, 4.50/3.82 = 1.178]

Fringe order	Left section $\theta = 90^\circ$		σ (lb/sq in.)	Right section $\theta = 270^\circ$	
	Distance from origin (in.)			Distance from origin (in.)	
	Photographic	Actual		Photographic	Actual
-4.5	0	0	-1330	0	0.
-4	.025	.029	-1180	.023	.027
-3	.070	.082	-885	.069	.081
-2	.115	.135	-590	.102	.120
-1	.160	.189	-295	.156	.184
0	.200	.236	0	.196	.231
1	.236	.278	295	.234	.276
2	.274	.323	590	.269	.307
3	.308	.363	885	.303	.357
4	.340	.400	1180	.334	.394
5	.380	.448	1475	.365	.430
6	.405	.477	1771	.398	.469

TABLE IV

VALUES OF σ' AND y' MEASURED FROM FIGURE 12

Distance from origin	y' (in.) (1)	σ' (lb/sq in.) (2)	$\sigma' y'$
0	-0.26	-1480	385
.04	-.22	-1270	280
.08	-.18	-1060	191
.12	-.14	-840	117
.16	-.10	-615	61.5
.20	-.06	-385	23
.24	-.02	-130	2.6
.28	.02	145	2.9
.32	.06	425	25.5
.36	.10	720	72
.40	.14	1030	144
.44	.18	1315	237
.48	.22	650	363

[1]The symbol y' represents distance from neutral axis.

[2]The symbol σ' represents stress due to bending only.

TABLE V

RESULTS OF TESTS ON CIRCULAR RINGS

SUPPORTED AS BULKHEADS IN MONOCOQUE SHELLS

[$\theta = 75°$]

Model	Test	Load, W (lb)	Skin thickness t (in.)	Mean diameter D_M (in.)	Ring depth, d (in.)	Cantilever span ℓ (in.)	Taper angle β (deg)	$\frac{M}{WR_M}$	$\frac{\ell}{D_M}$	$\frac{t}{d}$	Figure
2	6	76.00	0.020	1.998	0.260	0.38	2.5	0.0891	0.188	0.080	35
201	1	16.05	.010	2.017	.171	2.62	2.0	.1050	1.300	.058	36
201	1	20.60	.010	2.017	.171	2.62	2.0	.1038	1.300	.058	37
3	1a	72.70	.010	2.980	.360	.38	.0	.0945	.128	.028	38
3	1a	99.00	.010	2.980	.360	.38	.0	.0935	.128	.028	39
3	1	47.00	.015	2.980	.360	2.60	2.5	.1030	.872	.042	40
3	6	77.00	.020	2.980	.360	.72	2.5	.0997	.240	.056	41
3	5	47.00	.020	2.980	.360	1.10	2.5	.0983	.369	.056	42
3	4	47.00	.020	2.980	.360	1.10	2.5	.1015	.369	.056	43
3	4	77.00	.020	2.980	.360	1.10	2.5	.1015	.369	.056	44
3	5	77.00	.020	2.980	.360	1.10	2.5	.0984	.369	.056	45
3	6	91.10	.051	2.980	.360	.72	2.5	.0901	.240	.142	46
3	5	47.00	.051	2.980	.360	1.10	2.5	.0930	.369	.142	47
3	5	77.00	.051	2.980	.360	1.10	2.5	.0898	.369	.142	--
3	5	47.00	.082	2.980	.360	1.10	2.5	.0832	.369	.228	48
3	5	77.00	.082	2.980	.360	1.10	2.5	.0860	.369	.228	49
301	1	27.80	.015	3.013	.271	2.62	2.5	.1020	.870	.056	50
301	1	39.00	.015	3.013	.271	2.62	2.5	.1020	.870	.056	51
4	1	77.00	.020	4.005	.495	1.10	2.5	.0998	.275	.040	52
4	5	81.20	.020	4.005	.495	1.10	2.5	.0995	.275	.040	53
4	5	120.00	.020	4.005	.495	1.10	2.5	.0995	.275	.040	20
4	5	120.00	.051	4.005	.495	1.10	2.5	.0954	.275	.103	54
4	5	120.00	.082	4.005	.495	1.10	2.5	.0890	.275	.166	55
4	5	158.50	.164	4.005	.495	1.10	2.5	.0682	.275	.331	56
4a	1a	79.10	.010	3.970	.488	.38	.0	.0955	.096	.021	57
4a	1a	115.80	.010	3.970	.488	.38	.0	.0952	.096	.021	58
4a	5	120.00	.020	3.970	.488	1.10	2.5	.0987	.277	.040	59
4a	6	120.50	.020	3.970	.488	1.10	2.5	.0962	.277	.040	60
4a	6	139.20	.123	3.970	.488	1.10	2.5	.0800	.277	.123	61
401	1	47.10	.020	3.982	.353	2.62	2.5	.0974	.656	.057	62
401	1	62.00	.020	3.982	.353	2.62	2.5	.0963	.656	.057	63

TABLE VI

COMPUTATION OF CORRECTION FACTOR

TO BE APPLIED FOR SKIN SHEAR STRESS

(1)	(2)	(3)	(4)	(5)	(6)
θ	$\sin\theta$	$\left[1-(\pi-\theta)\ \sin\theta+\frac{1}{2}\cos\theta\right]$	$\frac{\text{Column (2)}}{\text{Column (3)}}$	$\tan\phi$ $\frac{d}{R}=\frac{1}{4}$	$\cos\phi$ $\frac{d}{R}=\frac{1}{4}$
0	0.000	-1.500	0.000	0.000	1.000
15	.259	.737	-.351	-.015	.999
30	.500	.123	-4.07	-.170	.989
45	.707	.307	2.30	.096	.992
60	.866	.560	1.54	.064	.995
75	.966	.644	1.48	.062	.995
90	1.000	.570	1.76	.073	.994
105	.966	.394	2.45	.102	.992
120	.866	.160	5.36	.223	.975
135	.707	-.091	-7.76	-.333	.945
150	.500	-.305	-1.64	-.068	.992
165	.259	-.449	-.59	-.025	.998
180	.000	-.500	-.00	.000	1.000

TABLE VII

MEASUREMENT OF LOCATION OF FRINGES, FROM FIGURE 20

[Model 4; test 5; skin thickness, 0.020 in.; diametrical load, 120 lb; origin on outside brundary of ring; mean photographic depth, 0.383 in.; mean actual depth, 0.495 in.; ratio of depths, 0.497/0.383 = 1.295]

Fringe order	Left section $\theta = 75^\circ$		Right section $\theta = -75^\circ$	
	Distance from origin (in.)		Distance from origin (in.)	
	Photographic	Actual	Photographic	Actual
-5.0	0	0	0	0
-4.0	.025	.0324	.033	.0427
-3.0	.061	.0790	.069	.0892
-2.0	.100	.1295	.107	.1385
-1.0	.132	.171	.145	.1875
0	.170	.220	.175	.226
1.0	.200	.259	.205	.265
2.0	.231	.299	.236	.305
3.0	.258	.334	.265	.343
4.0	.285	.369	.291	.376
5.0	.310	.401	.319	.4125
6.0	.336	.435	.342	.4425
7.0	.354	.458	.368	.476
8.0	.382	.495		

TABLE VIII

MOMENTS FOR CIRCULAR RING MODEL

[Model 4; test 5; skin thickness, 0.020 in.; diametrical load, 120.0 lb. See fig. 25.]

θ	$n_c + n_t$	Average $n_c + n_t$	$\frac{M}{WR_M}$	Corrected M/WR_M (1)	Theoretical M/WR_M (2)
0	-----	-----	------	-----	-0.238
0	-----	-----	------	-----	
15	-13.3	-13.15	-0.1005	-0.110	-.117
-15	-13.0				
30	-3.1	-3.20	-.024	-.026	-.020
-30	-3.3				
45	7.0	7.00	.054	.059	.049
-45	7.0				
60	11.6	11.40	.087	.095	.089
-60	11.2				
75	13.0	12.95	.099	.108	.102
-75	12.9				
90	11.8	11.75	.090	.098	.091
-90	11.7				
105	7.8	7.75	.059	.064	.063
-105	7.7				
120	4.0	3.50	.028	.031	.025
-120	3.0				
135	-1.5	-1.50	-.012	-.013	-.014
-135	-1.5				
150	-4.9	-5.00	-.038	-.042	-.049
-150	-5.1				
165	-8.1	-8.15	-.062	-.068	-.072
-165	-8.2				
180	-9.5	-9.50	-.073	-.080	-.080
-180	-9.5				

[1]Corrected by use of correction factor F from fig. 24.

[2]Theoretical values computed by use of equation from reference 2.

TABLE IX

MOMENTS FOR CIRCULAR RING AND FLOOR BEAM MODEL

[Model 8; total load, 61.2 lb]

θ	$n_c + n_t$	Average $n_c + n_t$	$\frac{M}{WR_M}$	Corrected M/WR_M	Theoretical M/WR_M (1)
0	10.2	10.2	0.042	0.045	0.036
0	10.2				
15	5.0	5.0	.021	.023	.024
-15	5.0				
30	-3.0	-2.5	-.010	-.011	-.009
-30	-2.0				
45	-22.0	-21.5	-.088	-.095	-.060
-45	-19.0				
60	----	----	----	----	-.121
-60	----				-.002
75	6.5	6.6	.027	.029	.034
-75	6.7				
90	11.2	11.1	.046	.050	.046
-90	11.0				
105	10.5	9.4	.039	.042	.042
-105	8.3				
120	5.0	4.7	.019	.021	.027
-120	4.5				
135	1.0	1.0	.004	.004	.006
-135	1.0				
150	-4.0	-4.3	-.018	-.019	-.012
-150	-4.5				
165	-6.5	-7.0	-.029	-.031	-.027
-165	-7.5				
180	-8.0	-8.0	-.033	-.036	-.031
-180	-8.0				

[1]Theoretical values taken from an unpublished paper by Wayne Weisner entitled "Monocoque Fuselage Braced Circular Ring Analysis" written in competition for United Air Line Scholarship Awards in 1940.

TABLE X

MOMENTS FOR MAIN-SPAR BULKHEAD MODEL

[Model 6; I_B/I_R = 1142; b/R_M = 2.50]

θ	$n_c + n_t$	Average $n_c + n_t$	$\frac{M}{WR_M}$	Corrected M/WR_M
75	6.0	6.0	0.016	0.017
-75	6.0			
90	-4.1	-4.1	-.011	-.012
-90	-4.1			
105	-8.0	-8.5	-.022	-.024
-105	-9.0			
120	-8.0	-8.0	-.021	-.023
-120	-8.0			
135	-3.8	-3.6	-.009	-.010
-135	-3.4			
150	2.2	2.1	.006	.006
-150	2.0			
175	5.5	5.5	.014	.015
-175	5.5			
180	7.0	7.0	.018	.019
-180	7.0			

TABLE XI

MOMENTS FOR ELLIPTIC RING MODEL

[Model 9; total load, 47.0 lb]

θ	$n_c + n_t$	Average $n_c + n_t$	$\frac{M}{W\sqrt{ab}}$	Corrected $\frac{M}{W\sqrt{ab}}$
5	17.0	16.5	-0.152	-0.165
-5	16.0			
15	8.6	8.05	-.074	-.081
-15	7.5			
30	-1.4	-1.80	.016	.018
-30	-2.2			
45	-5.0	-5.30	.049	.053
-45	-5.6			
60	-7.3	-7.30	.067	.073
-60	-7.3			
75	-7.4	-7.25	.067	.073
-75	-7.1			
90	-7.0	-7.35	.058	.063
-90	-5.7			
105	-5.0	-4.65	.043	.047
-105	-4.3			
120	-3.2	-3.00	.028	.030
-120	-2.8			
135	0.0	0.0	.000	.000
-135	0.0			
150	2.6	2.95	-.027	-.029
-150	3.3			
165	5.0	5.25	-.048	-.052
-165	5.5			
180	6.0	6.00	-.055	-.060
-180	6.0			

TABLE XII

MOMENTS FOR FLYING-BOAT BULKHEAD MODEL

[Model 7; total load, 115.2 lb]

θ	$n_c + n_t$	Average $n_c + n_t$	d	d^2	$\frac{M}{W\sqrt{A/\pi}}$	t/d	F	Corrected $\frac{M}{W\sqrt{A/\pi}}$
0	3.1	3.10	1.030	1.060	0.1288	0.019	0.98	0.1315
10	4.5							
-10	4.2	4.35	.850	.722	.1235	.024	.98	.1260
20	6.2							
-20	5.8	6.00	.700	.490	.1155	.029	.97	.1190
30	8.3							
-30	8.5	8.40	.585	.342	.1130	.034	.97	.1160
40	11.0							
-40	11.0	11.00	.440	.194	.0838	.046	.96	.0874
50	14.5							
-50	14.0	14.25	.295	.087	.0477	.068	.95	.0498
60	0.0							
-60	0.0	.00	.304	.092	.0000	.066	.95	.0000
70	-3.0							
-70	-3.0	-3.00	.480	.221	-.0261	.042	.96	-.0272
80	-13.0							
-80	-13.0	-13.00	.280	.078	-.0398	.071	.95	-.0419
100	-10.0							
-100	-9.0	-9.50	.255	.065	-.0243	.078	.94	-.0258
120	-4.0							
-120	-5.0	-4.50	.255	.065	-.0115	.078	.94	-.0122
140	-.0							
-140	-.0	.00	.260	.0676	.0000	.077	.94	.0000
150	3.1							
-150	2.0	2.55	.295	.087	.0087	.068	.95	.0091
160	5.5							
-160	3.7	4.60	.260	.0676	.0122	.077	.94	.0130
170	5.6							
-170	5.2	5.40	.255	.065	.0138	.078	.94	.0147
180	5.7	5.70	.250	.0625	.0146	.080	.93	.0157

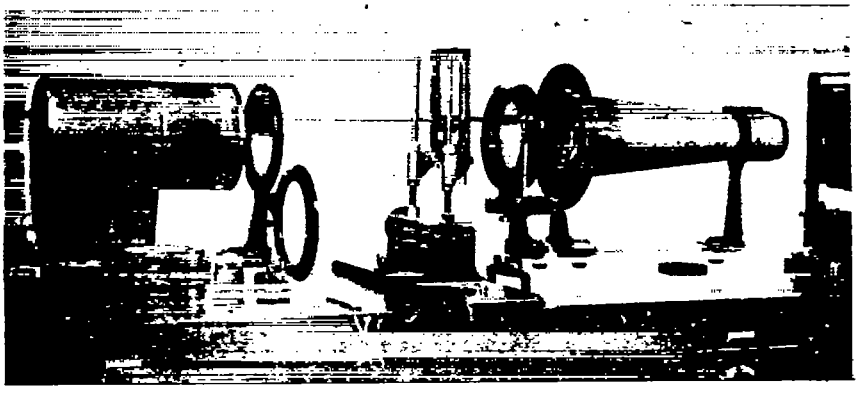

Figure 1.- Photoelastic polariscope.

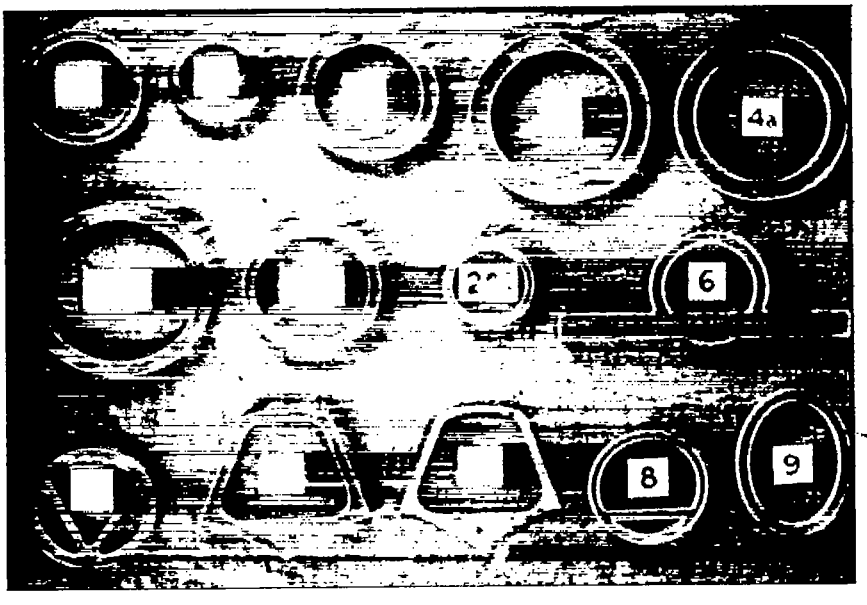

Figure 3.- Bulkhead models.

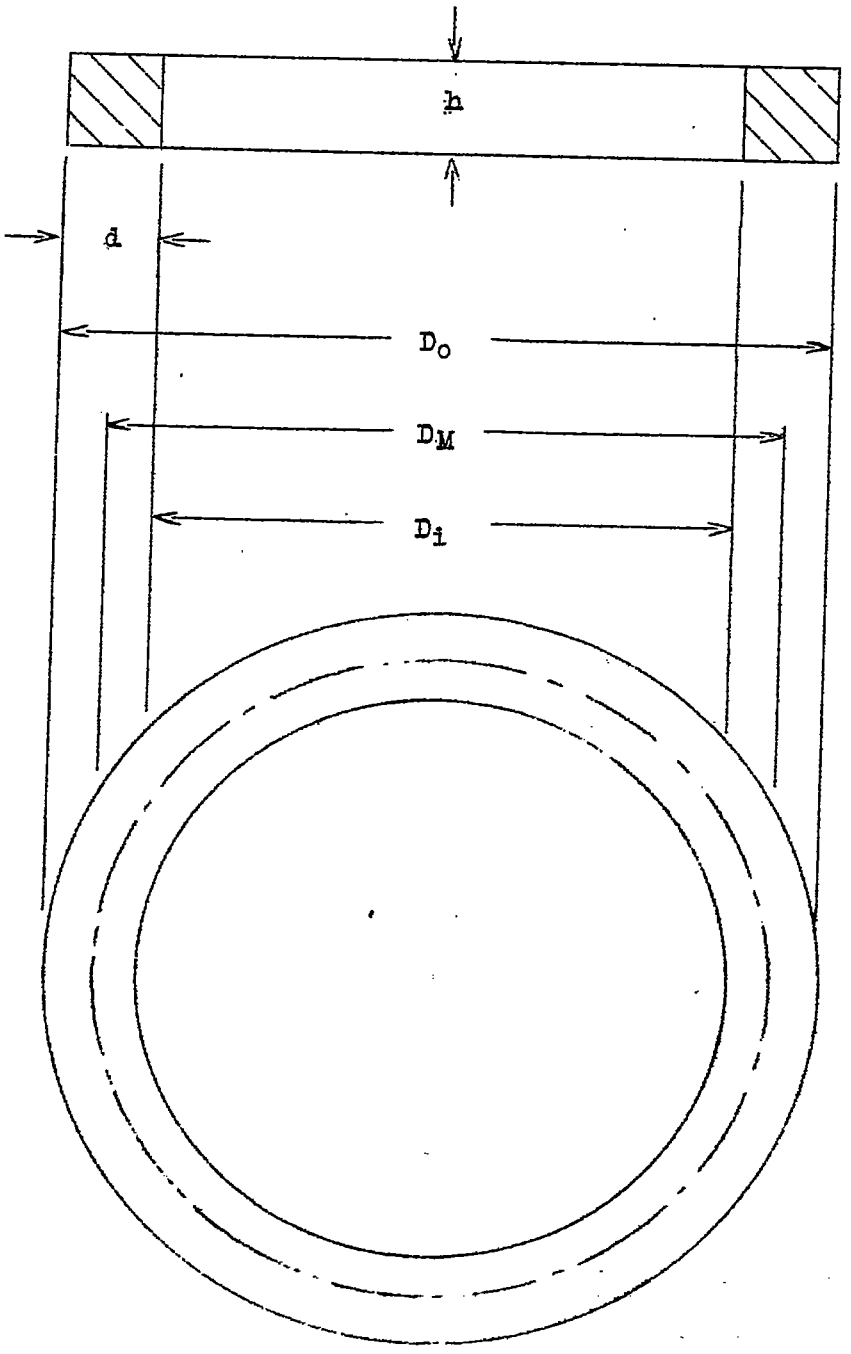

Figure 2.- Ring model dimensions.

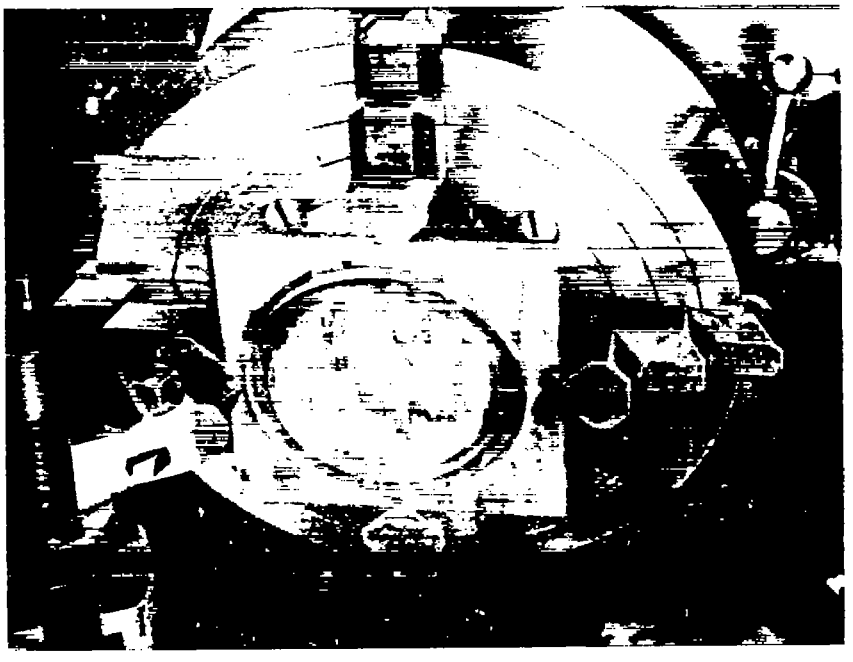

Figure 4.- Circular ring being cut in lathe.

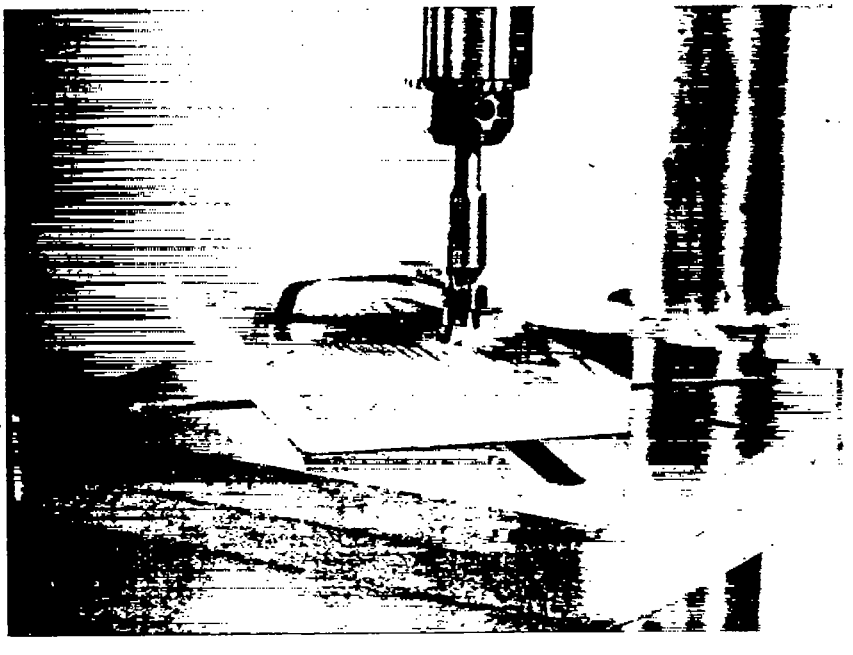

Figure 7.- Model being cut in vertical mill.

θ (deg)	r (in.)	d (in.)
0	1.38	1.030
10	1.33	.850
20	1.32	.700
30	1.35	.585
40	1.43	.440
50	1.56	.295
60	1.73	.304
70	1.84	.480
80	1.69	.280
100	1.50	.255
120	1.50	.255
140	1.72	.260
150	1.84	.295
160	1.86	.260
170	1.82	.255
180	1.81	.250

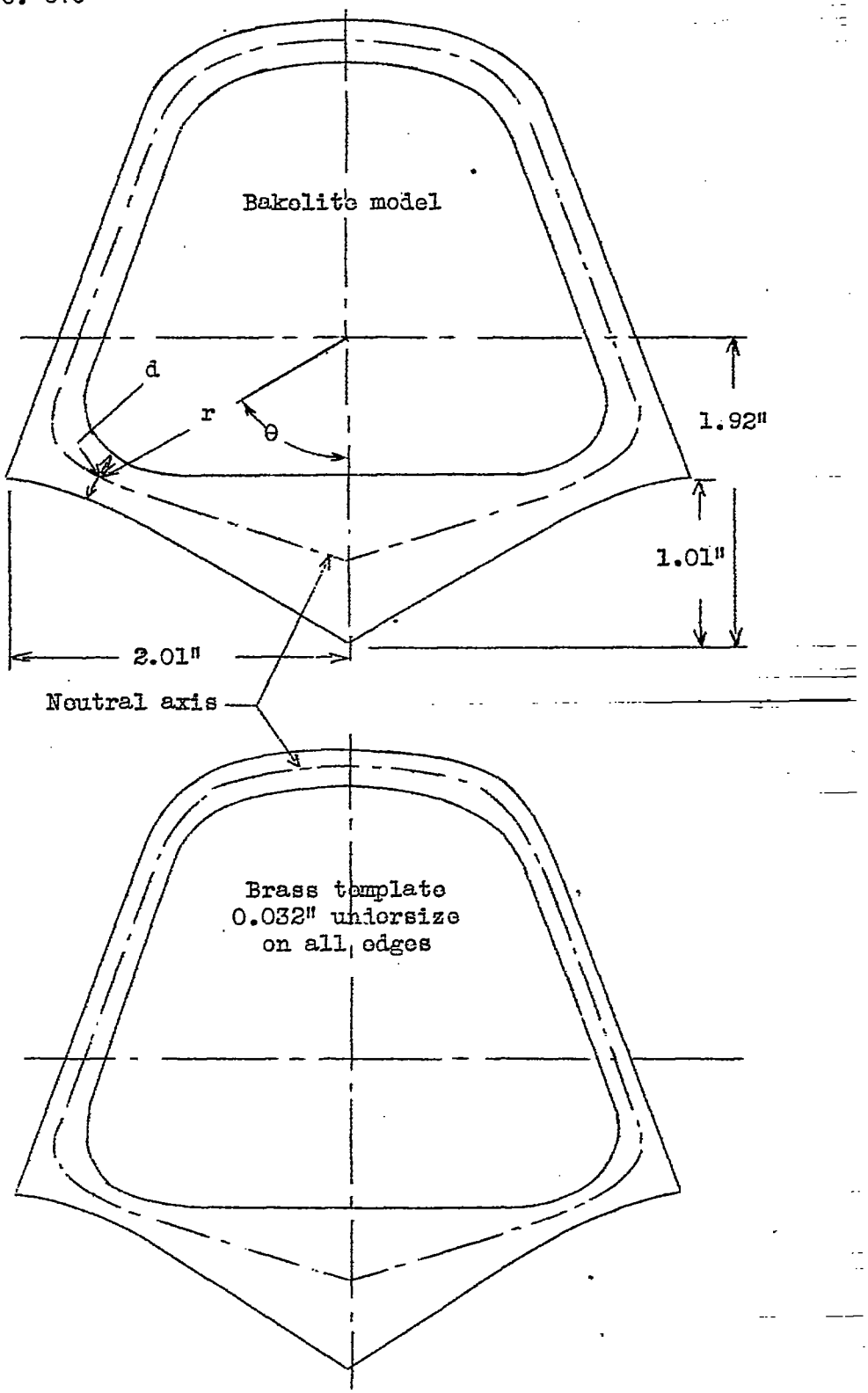

Figure 5.- Flying-boat bulkhead.

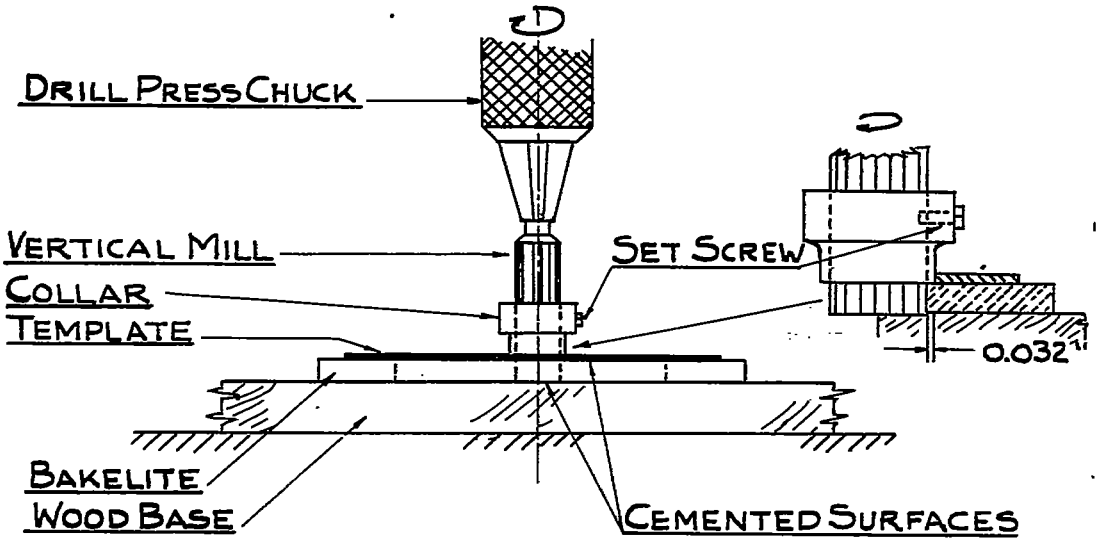

FIGURE 6.-METHOD OF MACHINING MODEL

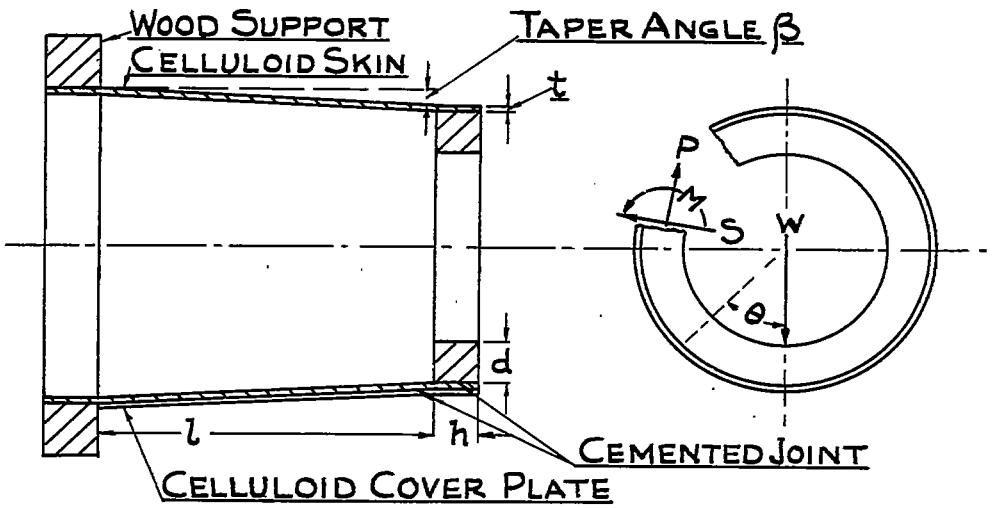

FIGURE 9

DETAILS OF MODEL MOUNTING

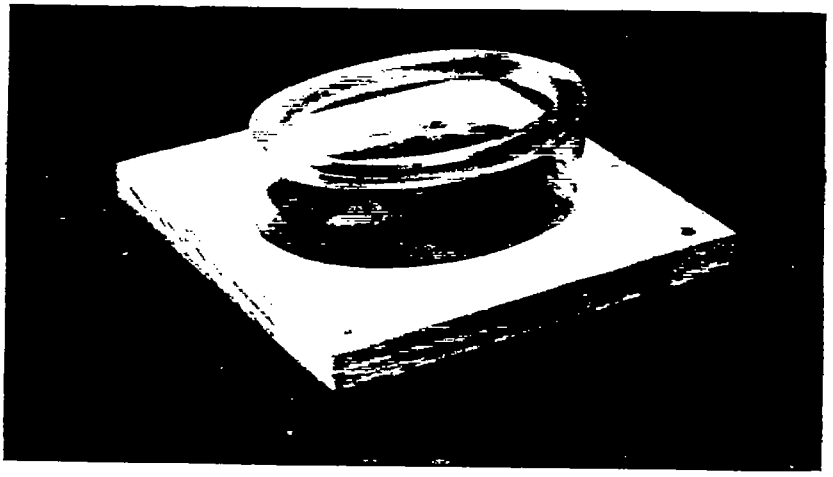

Figure 8.- Mounting of elliptic bulkhead model.

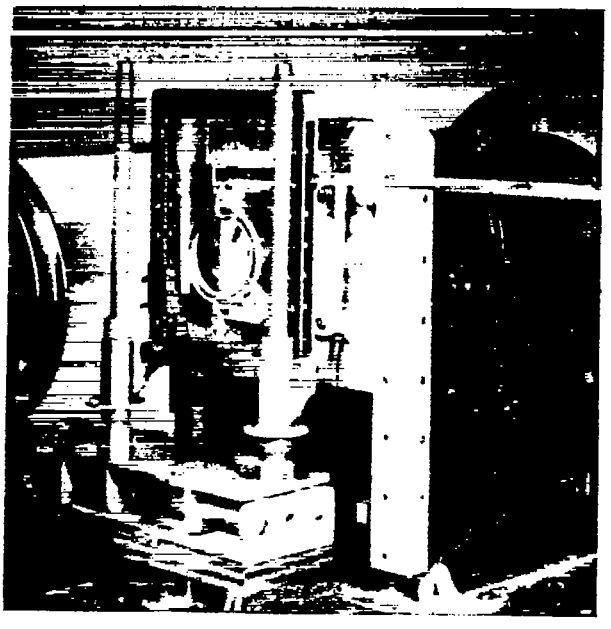

Figure 10.- Ring model loaded for test.

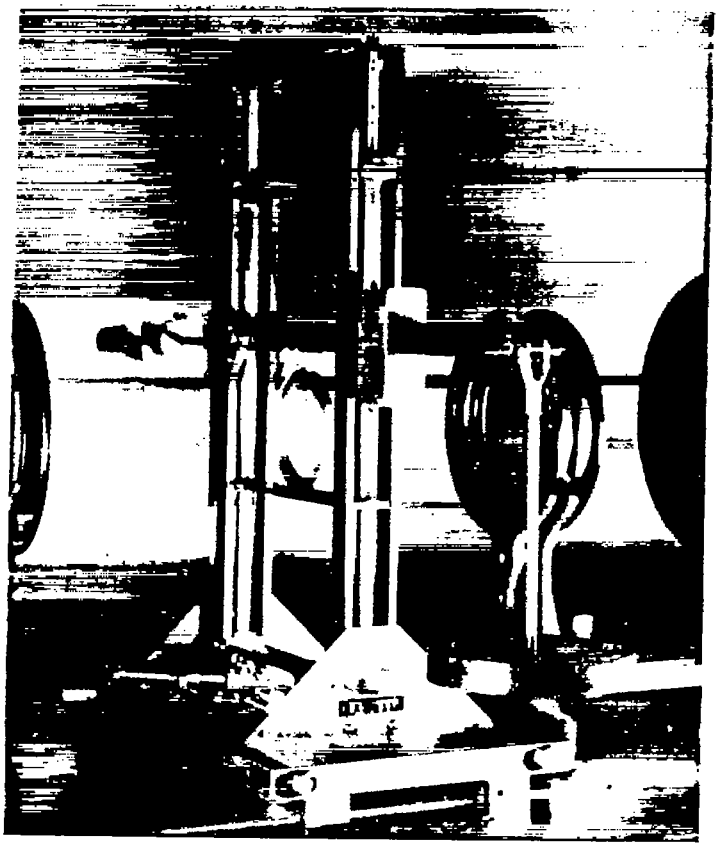

Figure 11.- Ring model under diametrical load.

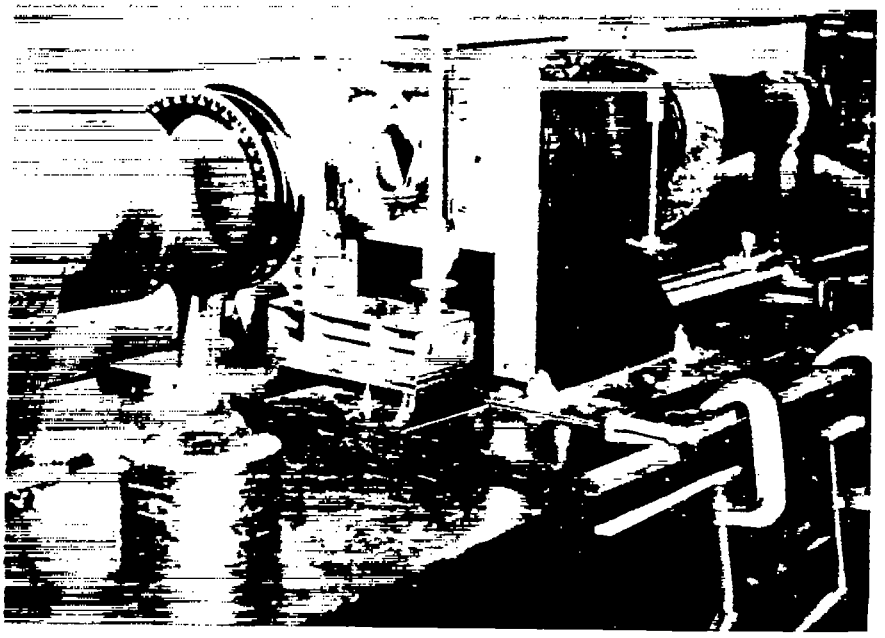

Figure 32.- Model 7 loaded for test.

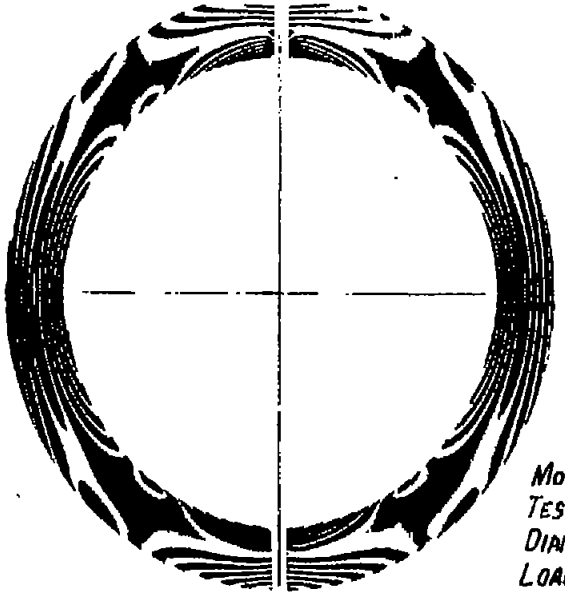

Figure 13.- Photoelastic fringe pattern for model 4, test 3. Diametrical load, 51.3 pounds.

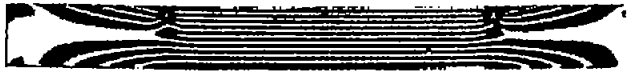

CALIBRATION BEAM
TEST No's. 3 AND 4

Figure 13.- Photoelastic fringe pattern for calibration beam loaded at quarter-span points.

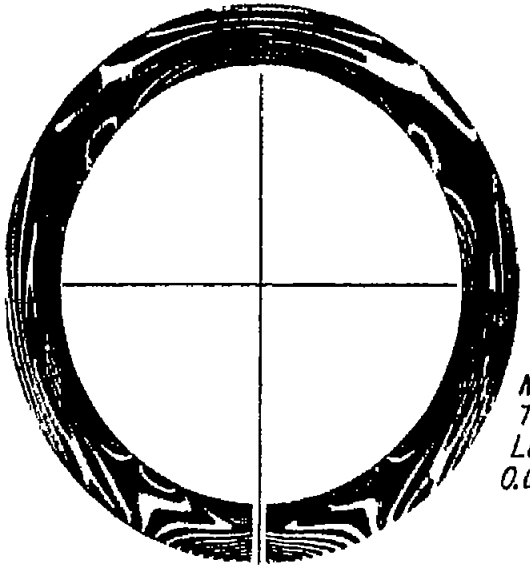

Figure 20.- Photoelastic fringe pattern for model 4, test 5. Skin thickness, 0.020 inch; diametrical load, 120 pounds.

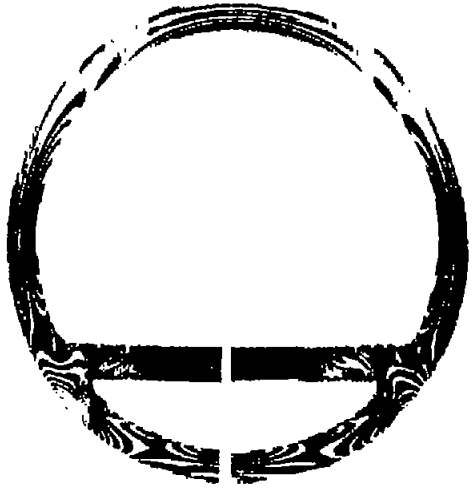

Figure 27.- Photoelastic fringe pattern for model 8. Total load, 61.2 pounds.

The black and white of the pattern is the reverse of the original.

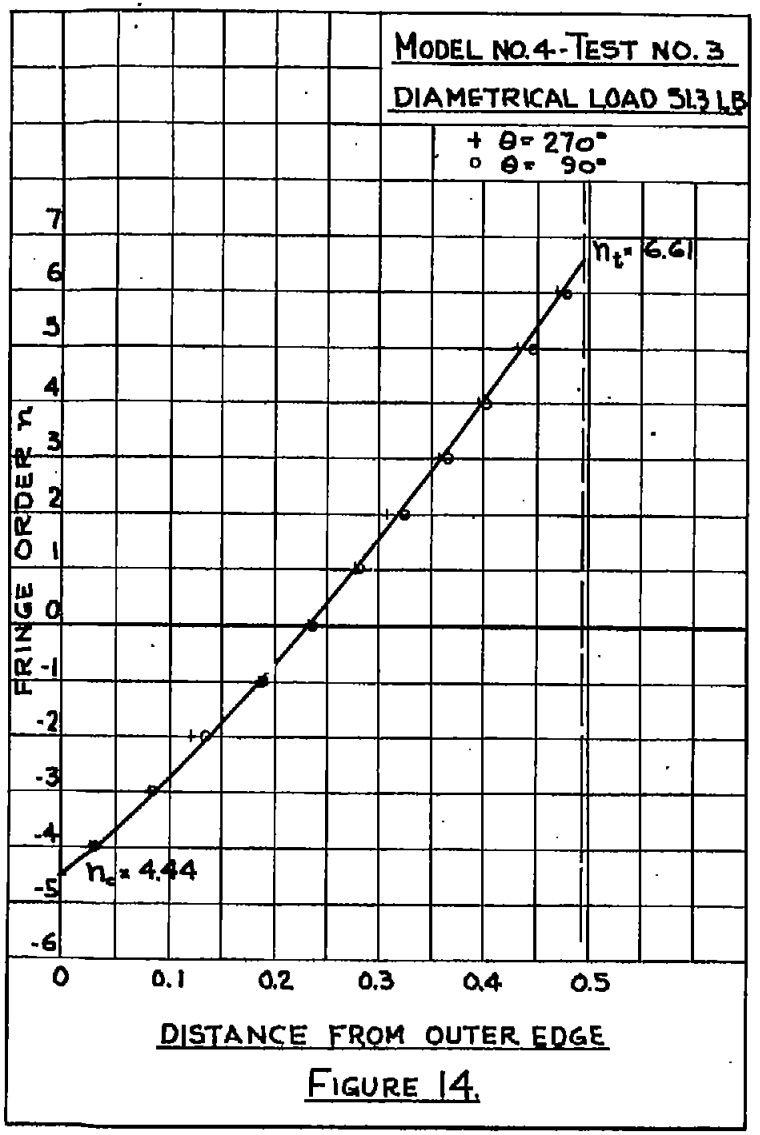

FIGURE 14.

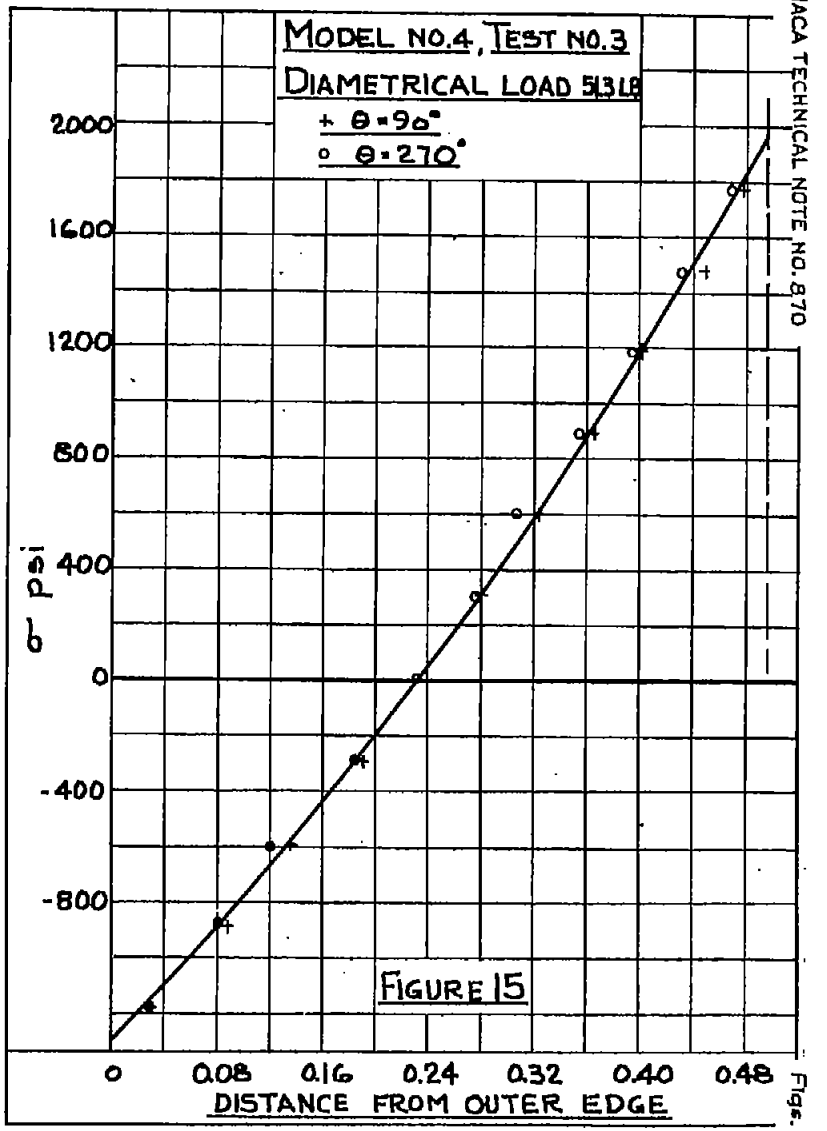

FIGURE 15

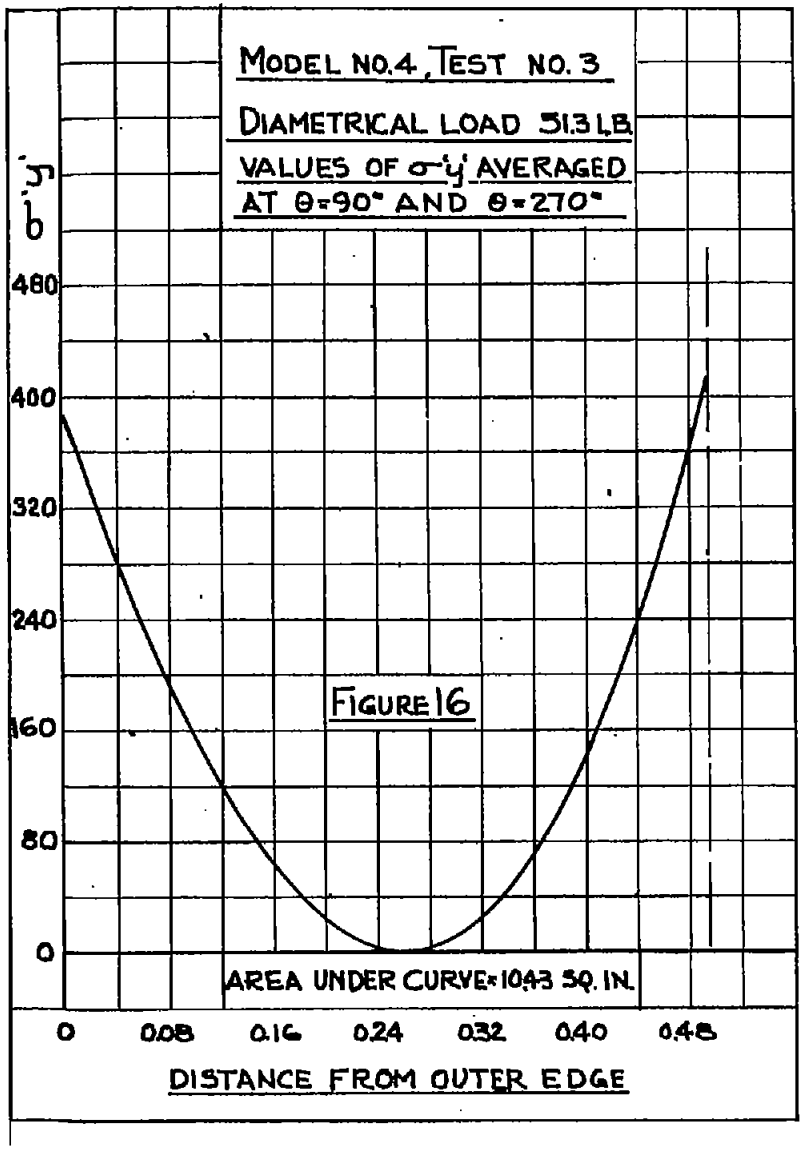

FIGURE 16

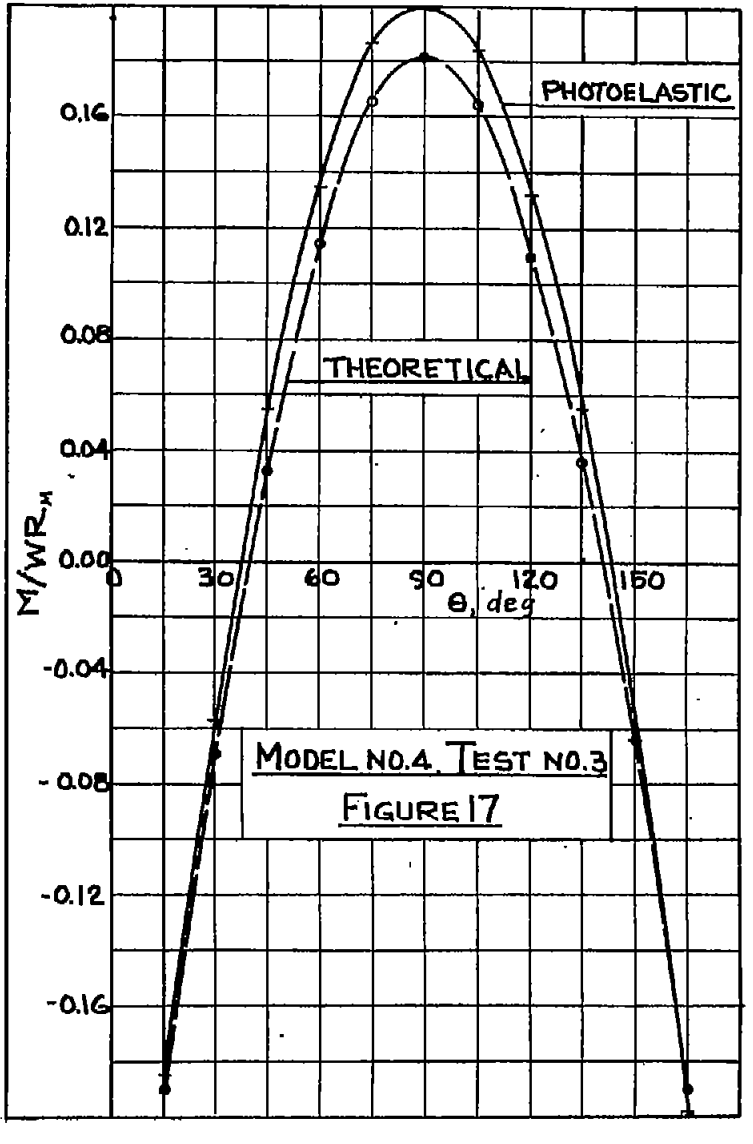

FIGURE 17

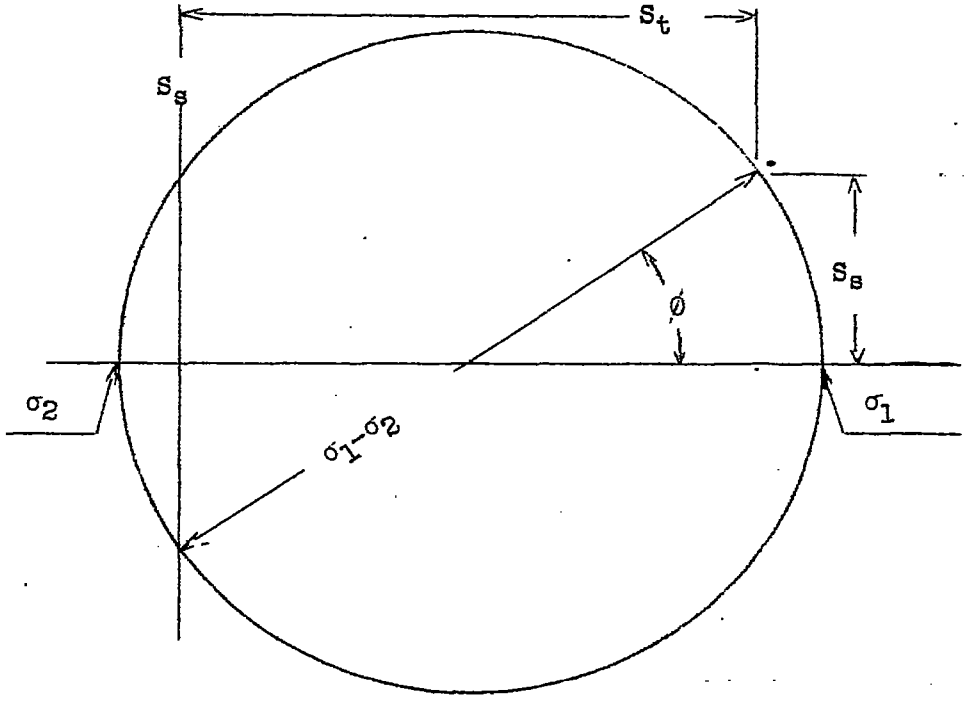

Figure 18.- Mohr's circle diagram of stress for edge of bulkhead attached to skin.

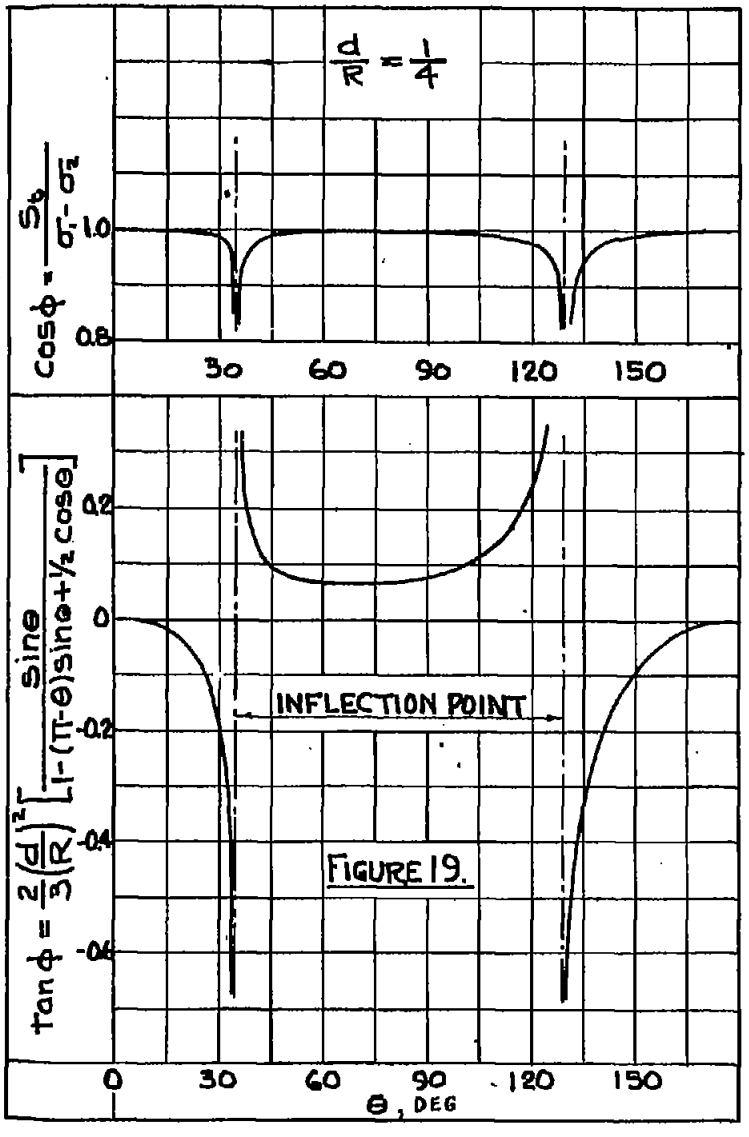

FIGURE 19.

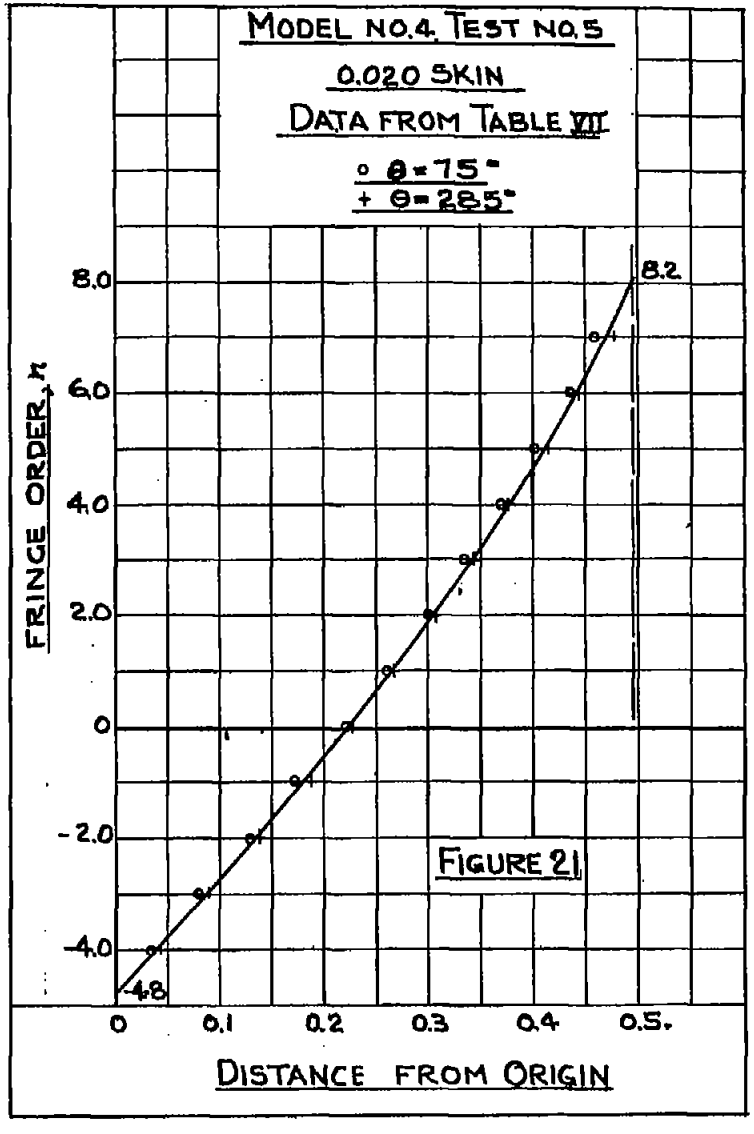

FIGURE 21

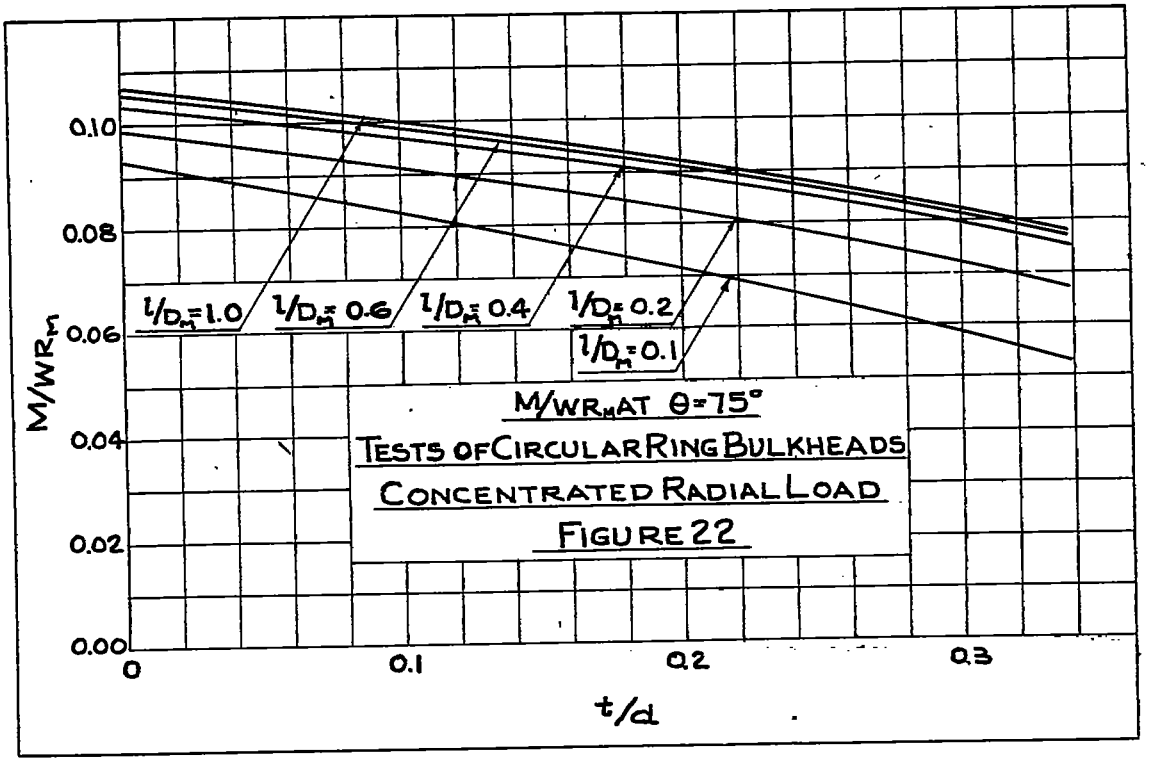
0.10
0.08
0.06
0.04
0.02
0.00
M/WR_M
0
0.1
0.2
0.3
t/d
l/D_M=1.0
l/D_M=0.6
l/D_M=0.4
l/D_M=0.2
l/D_M=0.1
M/WR_M AT θ=75°
TESTS OF CIRCULAR RING BULKHEADS
CONCENTRATED RADIAL LOAD
FIGURE 22

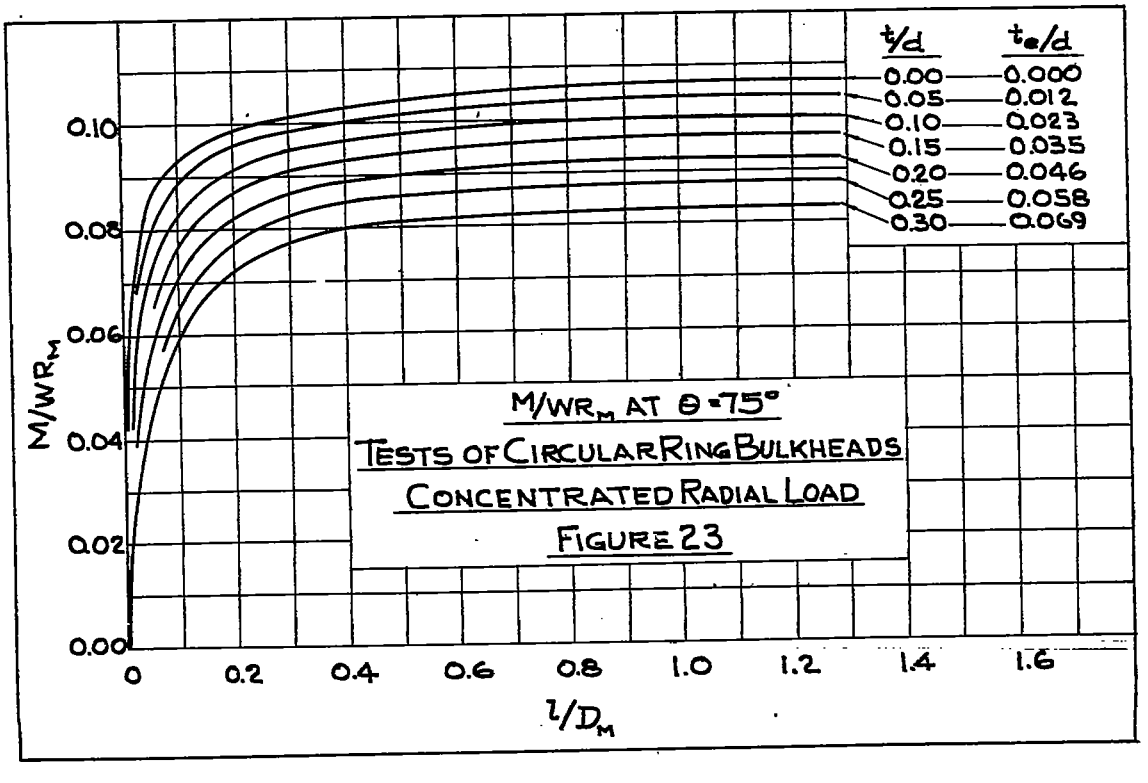
t/d
t_e/d
0.00 — 0.000
0.05 — 0.012
0.10 — 0.023
0.15 — 0.035
0.20 — 0.046
0.25 — 0.058
0.30 — 0.069
0.10
0.08
0.06
0.04
0.02
0.00
M/WR_M
0
0.2
0.4
0.6
0.8
1.0
1.2
1.4
1.6
l/D_M
M/WR_M AT θ=75°
TESTS OF CIRCULAR RING BULKHEADS
CONCENTRATED RADIAL LOAD
FIGURE 23

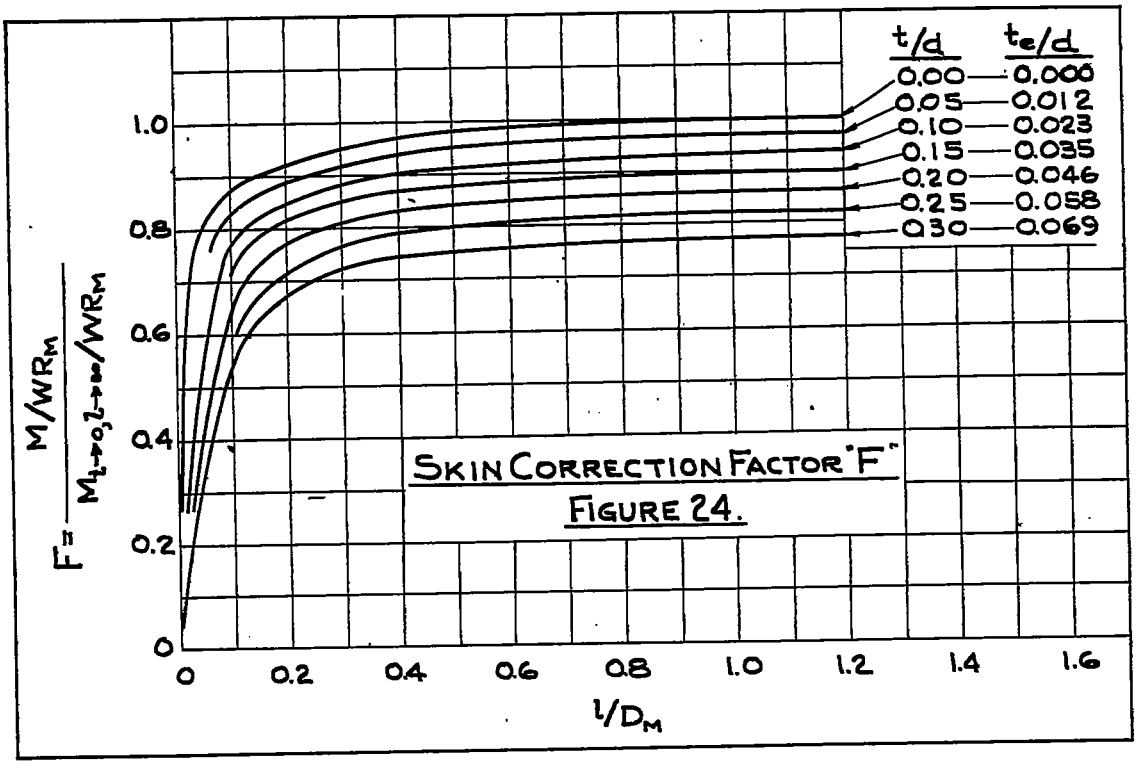

SKIN CORRECTION FACTOR "F"

FIGURE 24.

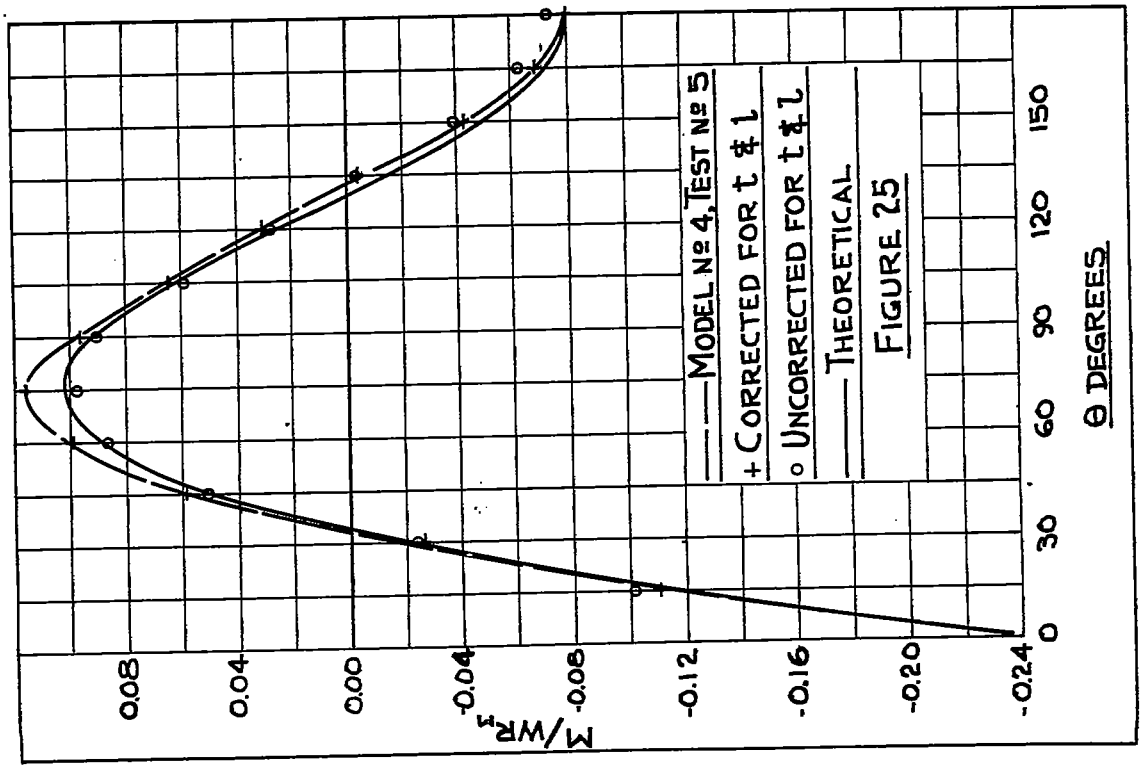

FIGURE 25

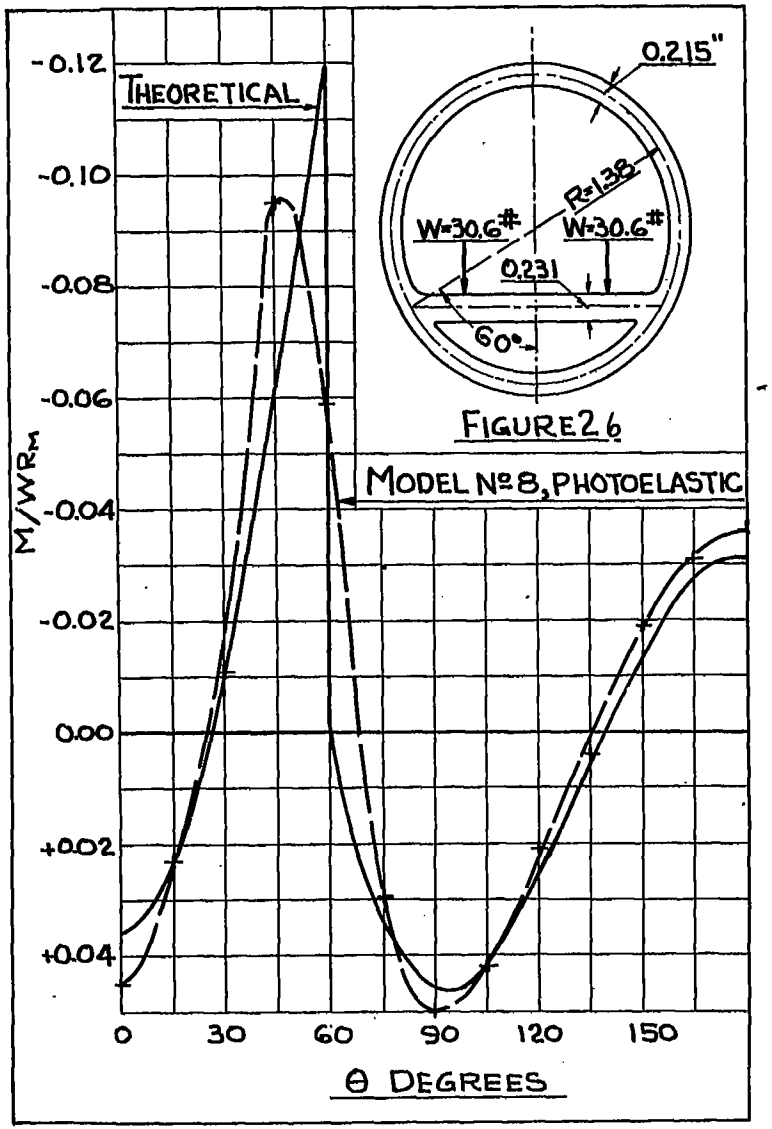

FIGURE 26

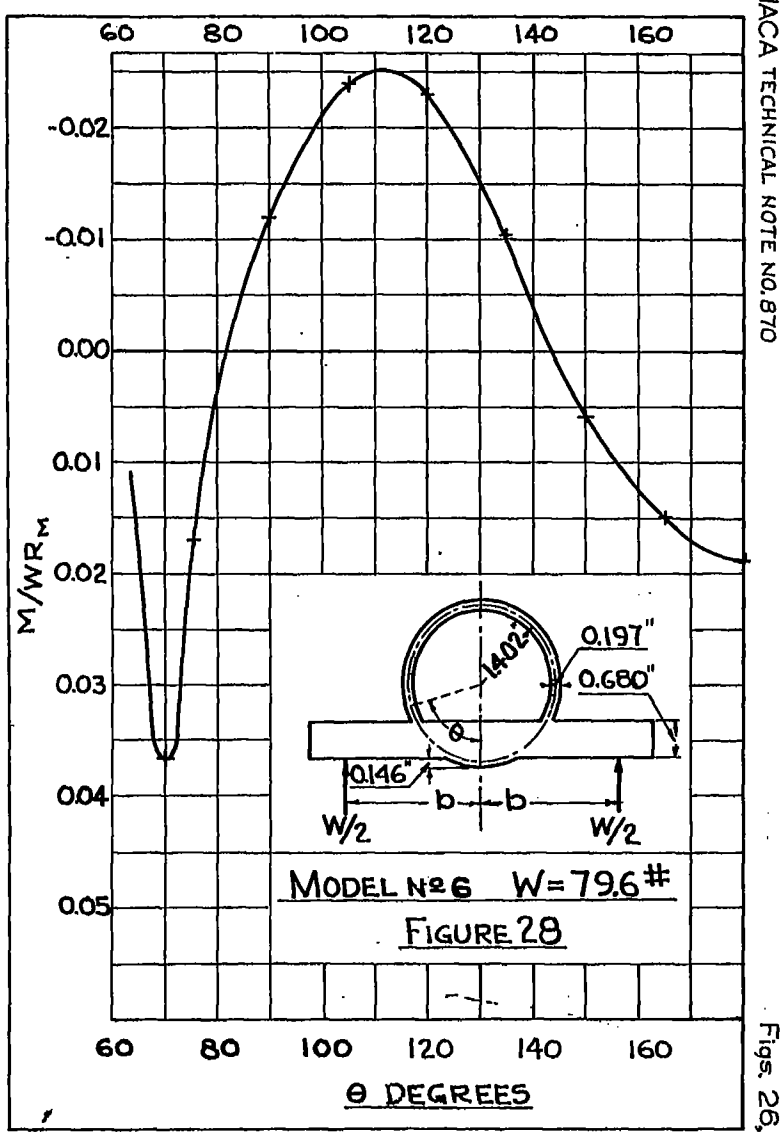

FIGURE 28

Figure 29.- Photoelastic fringe pattern for model 6.

Figure 31.- Photoelastic fringe pattern for model 8. Skin thickness, 0.020 inch; load, 47.0 pounds.

Figure 33.- Photoelastic fringe pattern for model 7. Load, 115.2 pounds.

Figure 35.- Model 2, test 6; skin thickness, 0.020 inch; load, 76.00 pounds.

The black and white of the pattern is the reverse of the original.

Figs. 29, 31, 33, 35

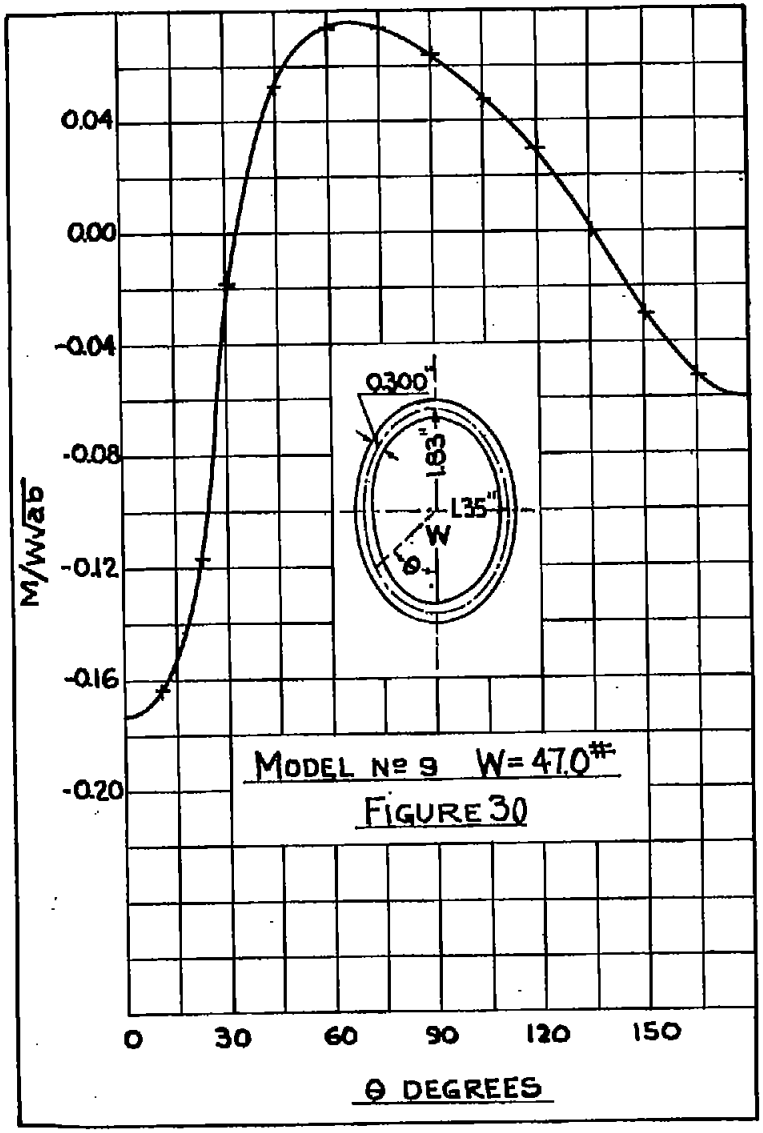

MODEL Nº 9 W=47.0#

FIGURE 30

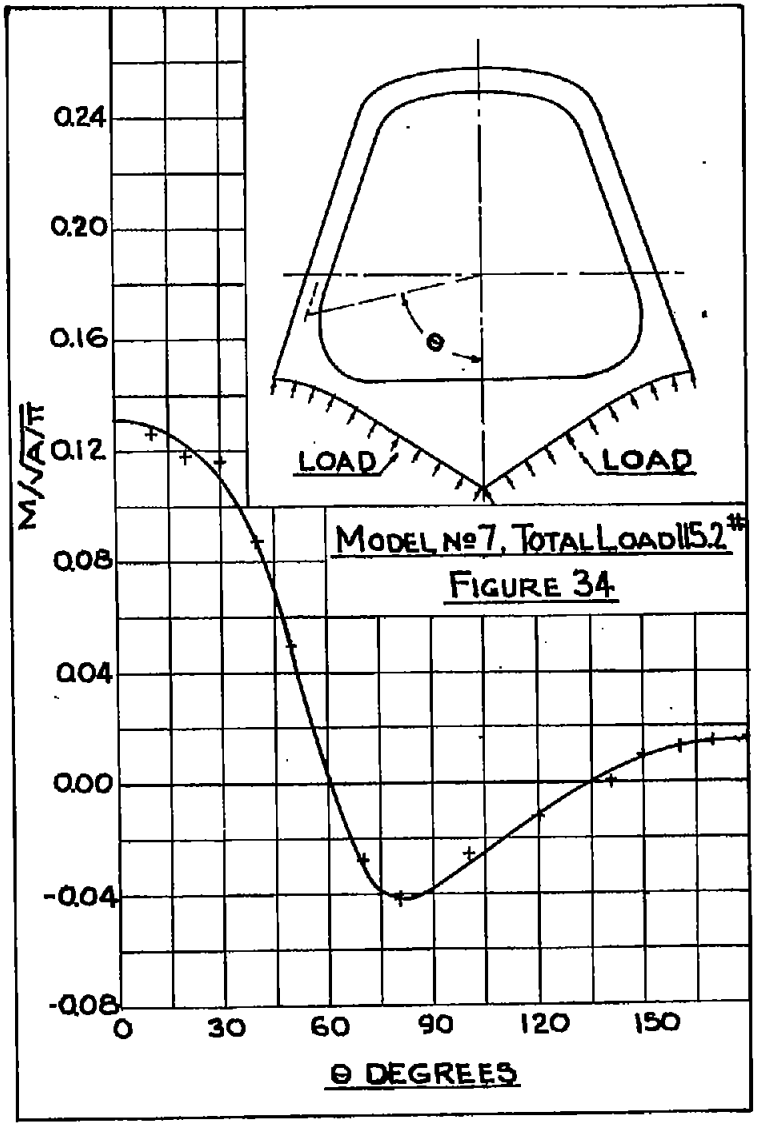

MODEL Nº 7, TOTAL LOAD 115.2#

FIGURE 34

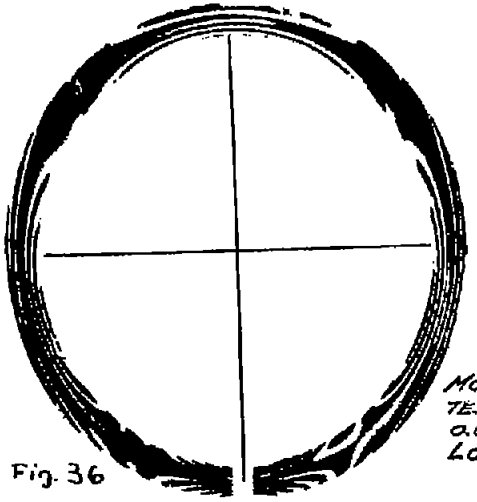

Fig. 36

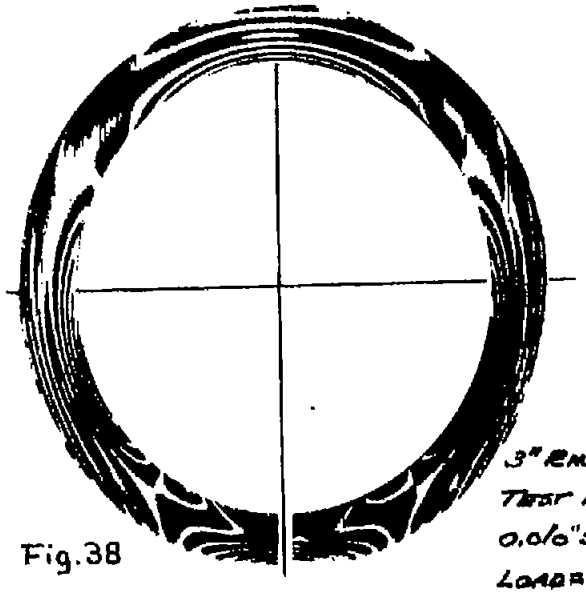

Fig. 38

The black and white of the pattern is the reverse of the original.

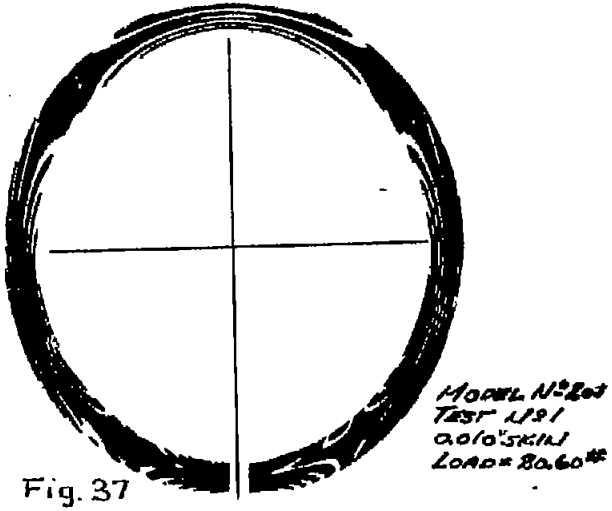

Fig. 37

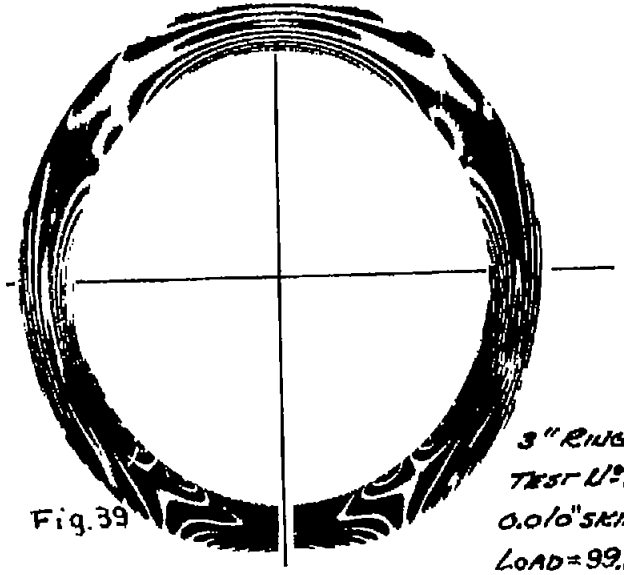

Fig. 39

Figs. 36, 37, 38, 39

Figures 36,37,38,39.- Photoelastic fringe patterns for circular rings tested. (See table V.)

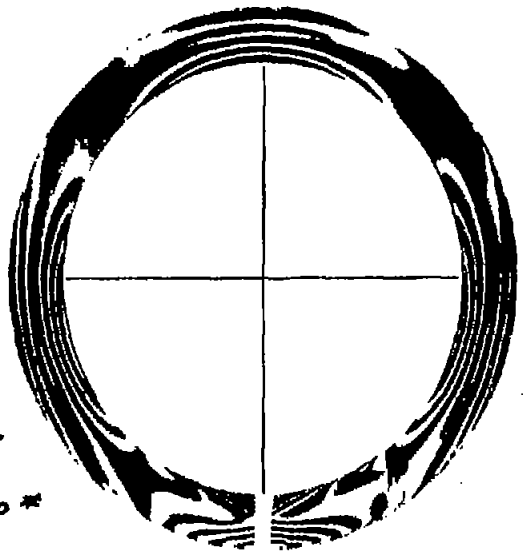

Fig. 40

MODEL No 3
TEST No 1
LOAD = 47.0 #
.015" SKIN

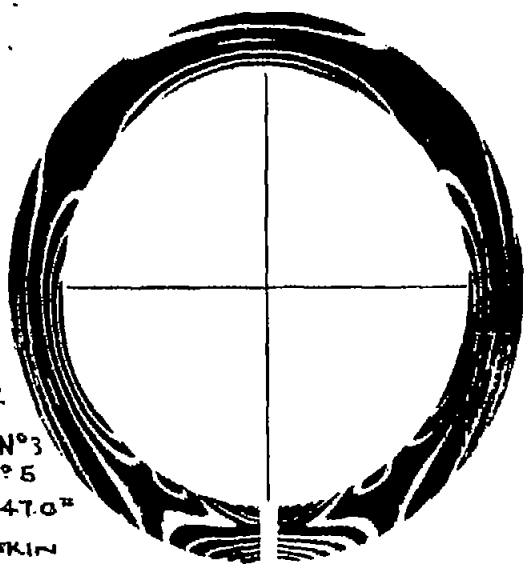

Fig. 42

MODEL No 3
TEST No 5
LOAD = 47.0 #
0.020" SKIN

The black and white of the pattern is the reverse of the original.

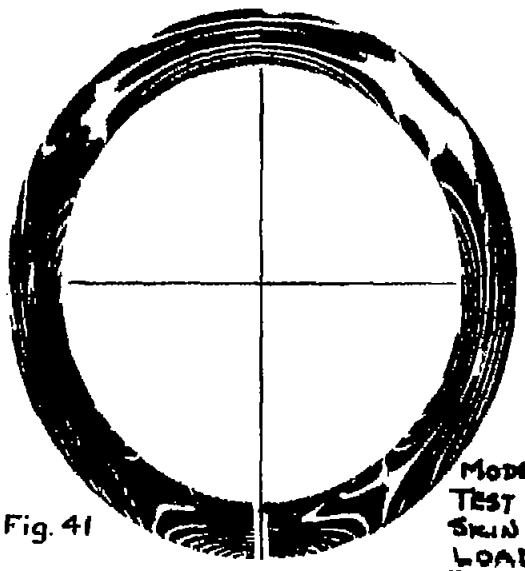

Fig. 41

MODEL No 3
TEST No 6
SKIN 0.020"
LOAD 77 #

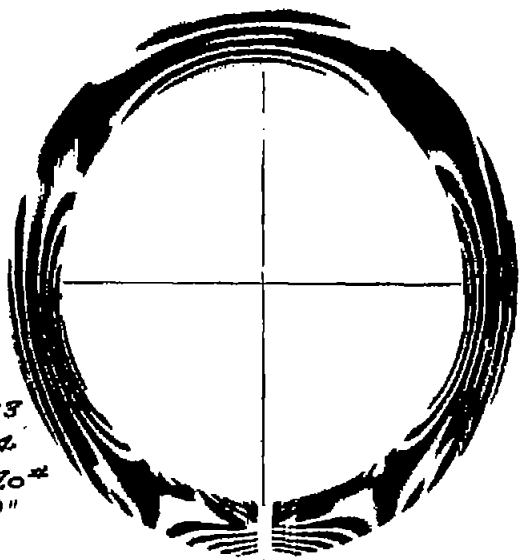

Fig. 43

MODEL No 3
TEST No 4
LOAD = 47.0 #
SKIN 0.020"

Figs. 40, 41, 42, 43

Figures 40,41,42,43.- Photoelastic fringe patterns for circular rings tested. (See table V.)

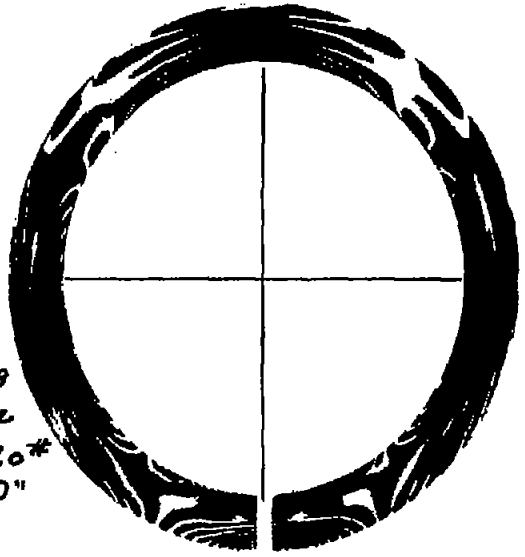

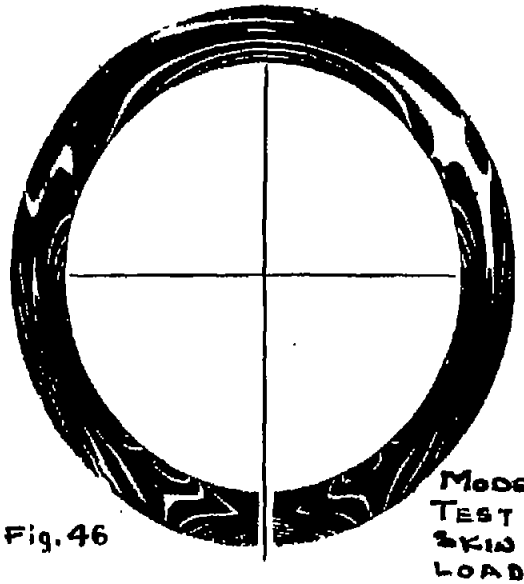

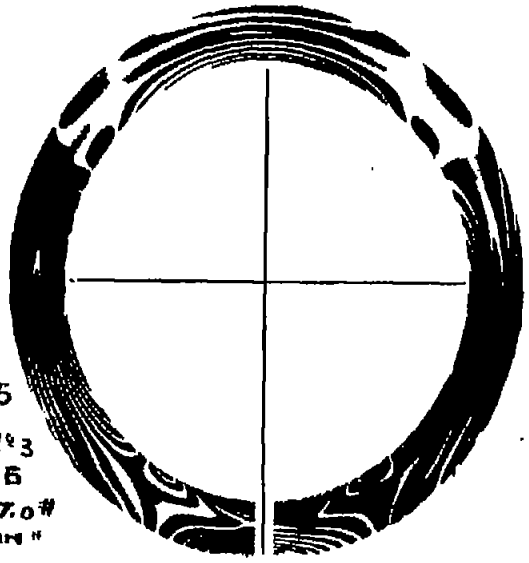

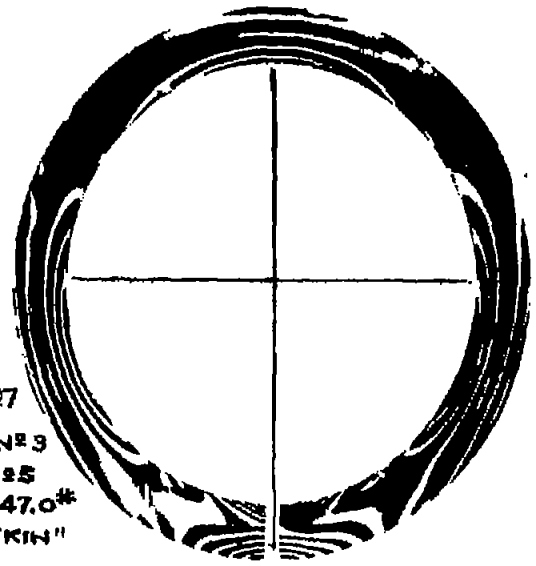

The black and white of the pattern is the reverse of the original

Figures 44,45,46,47.- Photoelastic fringe patterns for circular rings tested. (See table V.)

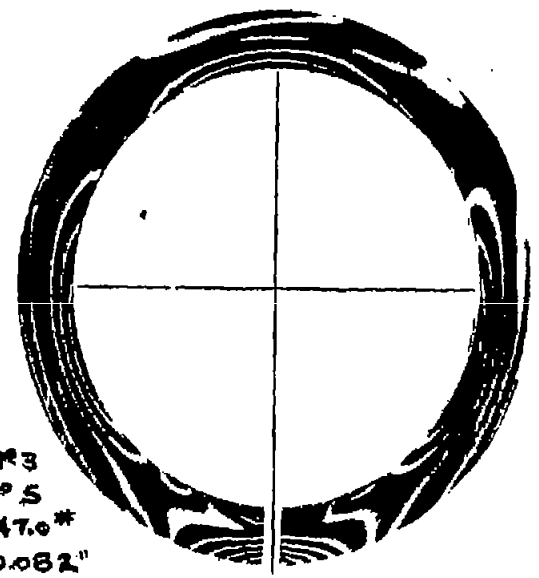

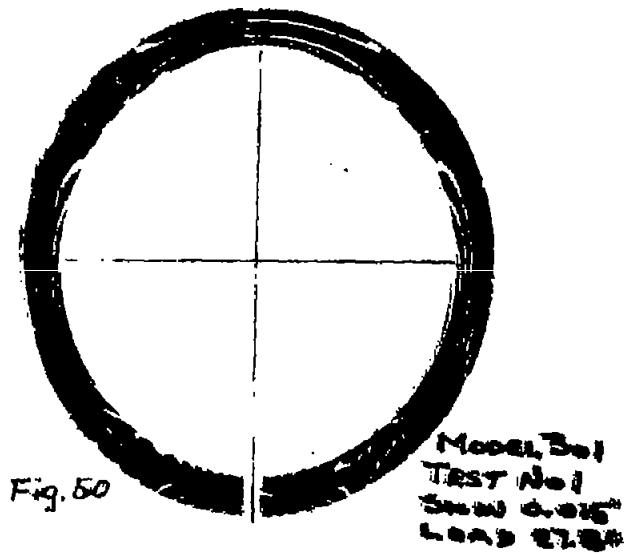

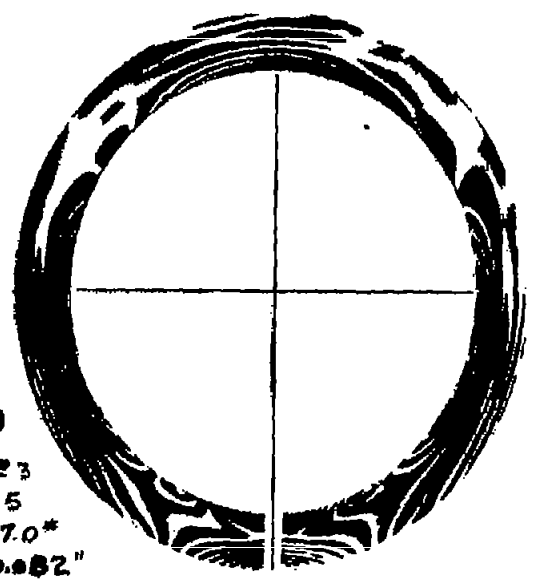

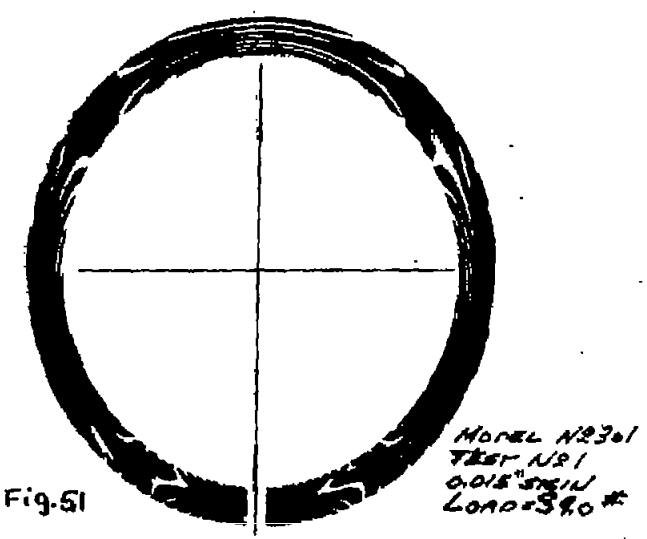

The black and white of the pattern is the reverse of the original.

Figures 48,49,50,51.- Photoelastic fringe patterns for circular rings tested. (See table V.)

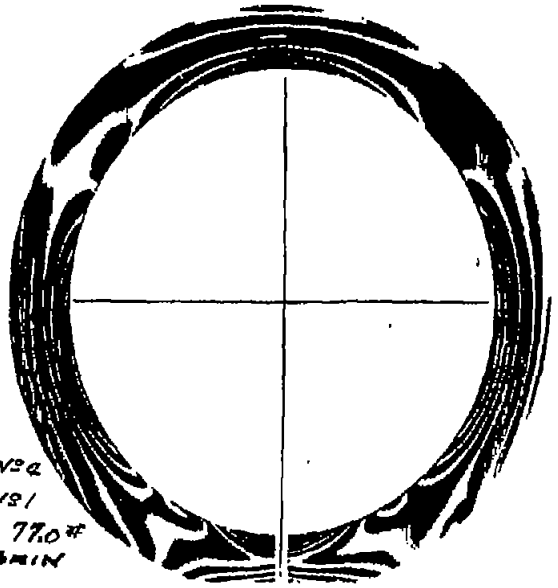

Fig. 52
MODEL Nº 2
TEST Nº 1
LOAD = 77.0 #
0.020" SKIN

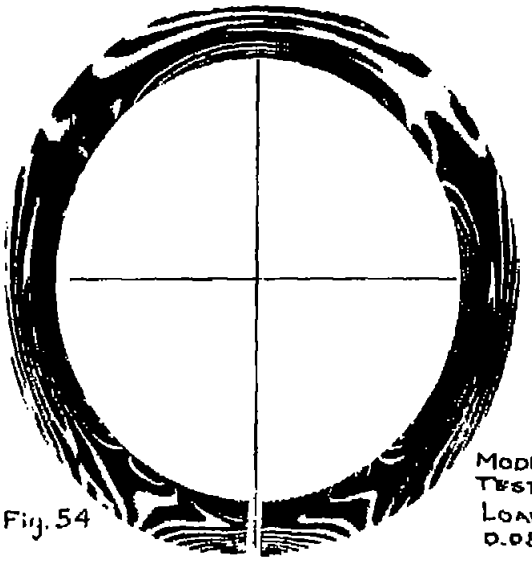

Fig. 54
MODEL Nº.
TEST Nº 5
LOAD = 120.
0.051" SKIN

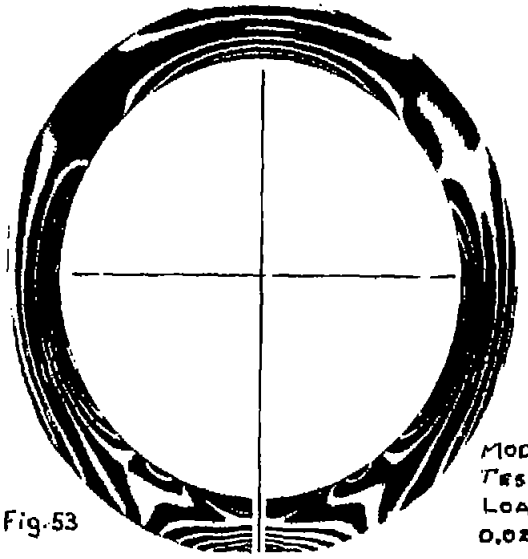

Fig. 53
MODEL Nº 4
TEST Nº 5
LOAD = 81.2 #
0.020" SKIN

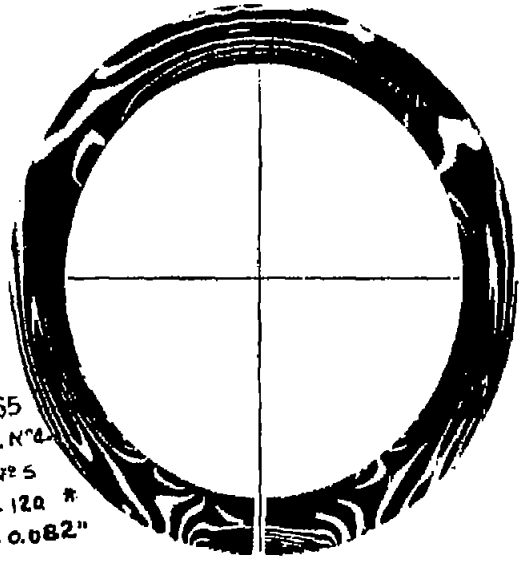

Fig. 55
MODEL Nº 4
TEST Nº 5
LOAD = 120 #
SKIN = 0.082"

he
lack
nd
hite
f the
attern
s the
everse
f the
riginal.

Figs. 52,53,54,55

Figures 52,53,54,55.- Photoelastic fringe patterns for circular rings tested. (See table V.)

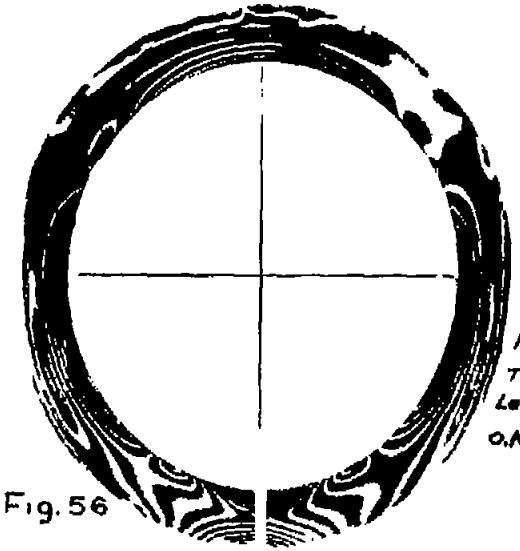

Fig. 56

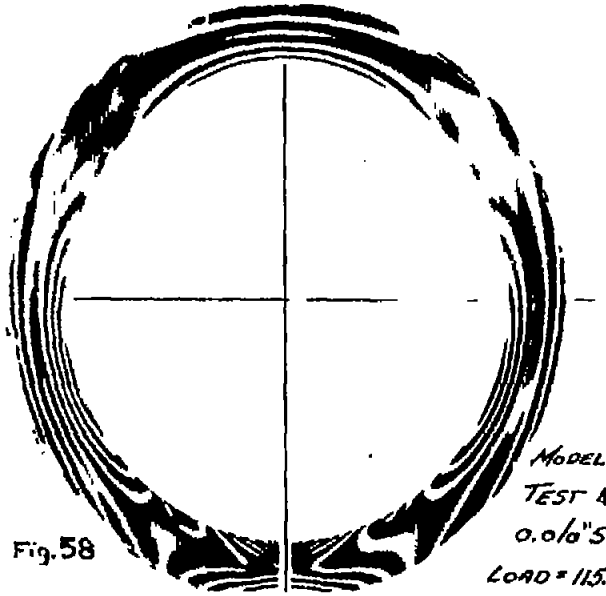

Fig. 58

The black and white of the pattern is the reverse of the original.

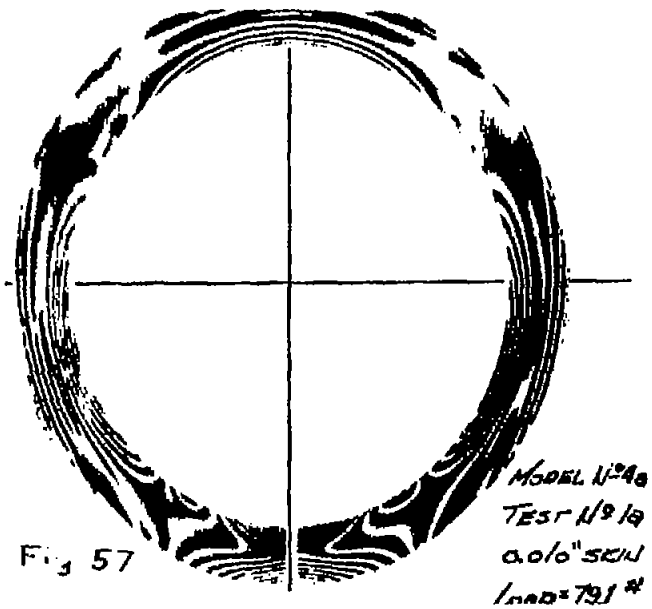

Fig. 57

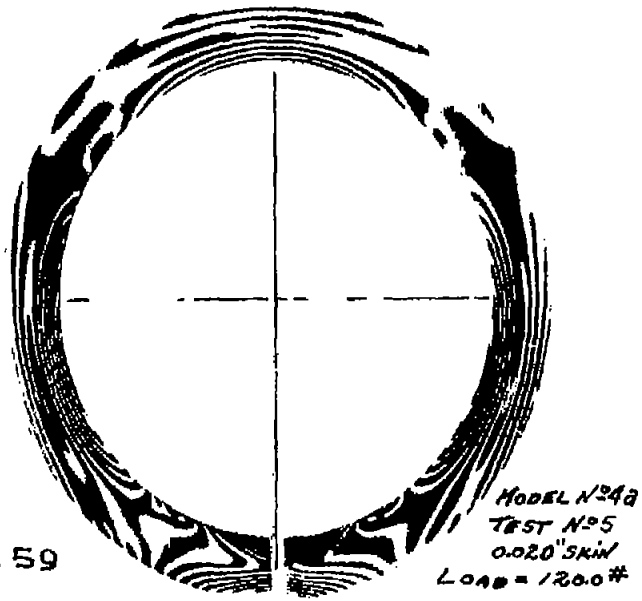

Fig. 59

Figs. 56,57,58,59

Figures 56,57,58,59.- Photoelastic fringe patterns for circular rings tested. (See table V.)

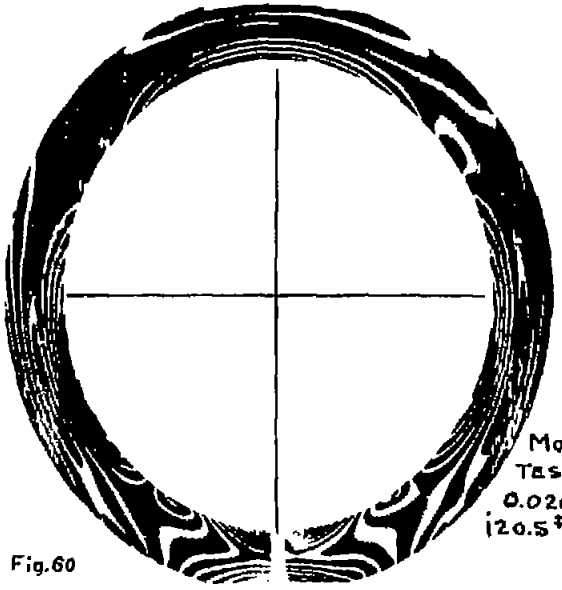

Fig. 60

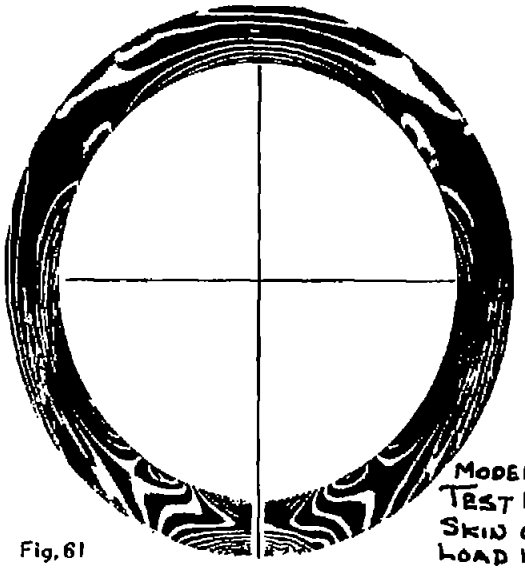

Fig. 61

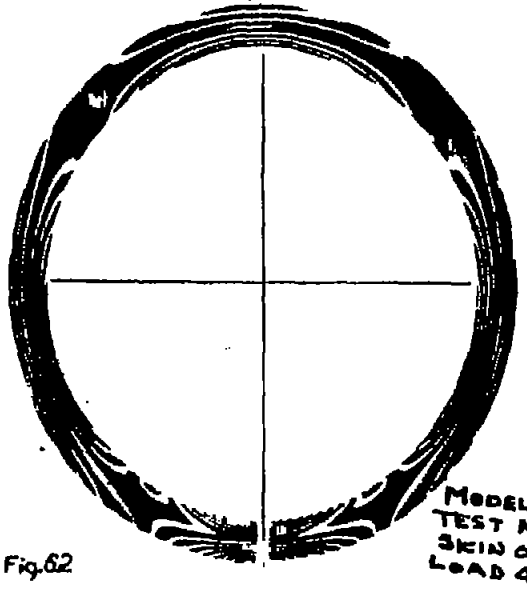

Fig. 62

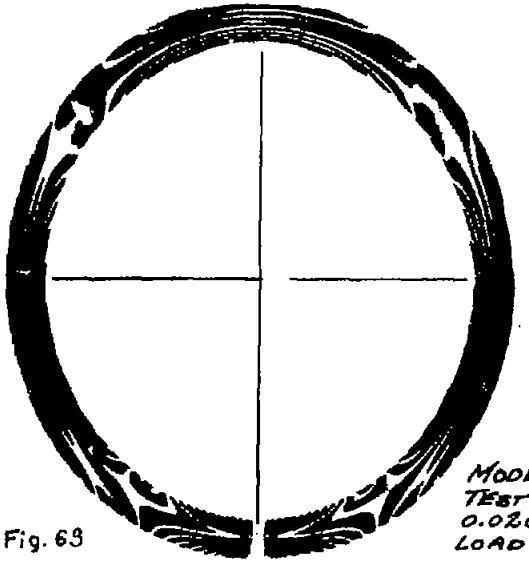

Fig. 63

The black and white of the pattern is the reverse of the original.

Figures 60,61,62,63.- Photoelastic fringe patterns for circular rings tested. (See table V.)